Chapter-6

Comparison of the cooking quality of developed meat analogue with existing soy-based product

6.1.Introduction

Meat analogues are increasingly popular plant-based products with distinctive textures and other characteristics, and are gaining traction in Asia, America and Europe (Bakr et al., 2023). The intensive production of traditional meat products has raised significant environmental concerns, including greenhouse gas emissions, deforestation, and water pollution (Djekic, 2015). Food safety issues, including bacterial contamination, antibiotic resistance, and zoonotic diseases have also become major concerns related to conventional meat consumption. Furthermore, growing awareness of health implications, animal welfare, environmental sustainability, and the movement towards plant-based diets has accelerated the development of meat alternatives (Boukid et al., 2024). The development and commercialization of plant-based meat alternatives (PBMA) could potentially address these concerns. In recent research, PBMAs have been successfully developed using pea protein and wheat gluten, effectively mimicking the texture of traditional meat products (McClements & Grossmann, 2021). Deep-fat frying has emerged as one of the most promising processing methods for the commercialization of PBMA products, particularly in the fast-food sector (Jang & Lee, 2024).

Deep-fat frying represents a cornerstone technique in both domestic cooking and commercial food production, particularly in the fast-food industry (Mahmud et al., 2023). This cooking method has gained widespread popularity due to its ability to impart distinctive flavors and create visually appealing products that satisfy consumer preferences (Saguy & Dana, 2003; De Angelis et al., 2024). The hallmark characteristic of deep-fried foods, their crispy texture, has become increasingly sought after by consumers worldwide, contributing to the continued dominance of this cooking method in both household and industrial settings (Mahmud et al., 2023). The process of deep-fat frying involves two critical mass transport phenomena: moisture loss and fat absorption. These fundamental processes can be manipulated through modifications to both the raw material properties and frying conditions, allowing producers to optimize the quality and nutritional characteristics of their products. Recent research has demonstrated significant

advances in controlling these parameters. For instance, Mohammadalinejhad & Dehghannya (2018) achieved a remarkable 23.18% reduction in fat absorption in potato chips through ultrasound pretreatment, while Bouchon & Dueik (2018) reported an impressive 50% reduction in oil content for carrot crisps using vacuum frying techniques. Additionally, Kita (2014) established that higher frying temperatures resulted in enhanced crispiness and more delicate texture profiles in French fries and potato crisps.

The cooking method employed in food preparation significantly influences the final product's quality attributes, including texture, moisture content, appearance, and sensory acceptability (Simpson et al., 2013). While traditional thermal methods like frying create desirable sensory characteristics through Maillard reactions and caramelization, they can potentially lead to higher fat content and the formation of acrylamide in certain foods (McClements & Grossmann, 2021; Boukid et al., 2024). In contrast, microwave cooking offers advantages in terms of speed and convenience, but may result in different moisture distribution patterns and textural properties due to its non-uniform heating mechanism (Simpson et al., 2013).

Understanding the kinetics of mass transfer during frying is crucial for predicting quality changes and optimizing product value through careful selection of frying conditions (Kita, 2014). The scientific literature contains numerous studies examining deep-fat frying modelling across various food products (Costa & Oliveira, 1999). Researchers have proposed several mathematical models to describe mass transfer during deep-fat frying, including first-order kinetic models and second-order polynomial models specifically for fat absorption (Kumar et al., 2022).

Texturized proteins have emerged as a popular plant-based ingredient, characterized by their versatile texture-forming capabilities and meat-like fibrous structure when properly processed. The application of protein structuring techniques serves multiple purposes: creating organized protein matrices that simulate muscle fiber architecture and developing products with meat-like mouthfeel and juiciness (Sivaranjani et al., 2024). These properties make texturized proteins especially suitable for deep-fat frying applications, where the protein structure helps maintain moisture and protect the product's integrity during high-temperature processing. Recent research efforts have

focused on developing optimized texturized proteins formulations suitable for large-scale manufacturing, with notable success achieved through novel protein blending and processing techniques (Gao et al., 2022; De Angelis et al., 2024).

Despite significant advances, a key research gap exists regarding mass transfer kinetics in fried texturized proteins. This study addresses this limitation by examining moisture loss and fat absorption kinetics in texturized protein-based meat alternatives at three different frying temperatures, focusing on how the unique protein matrix structure affects mass transfer phenomena. The research also compares quality parameters between conventional frying (160 °C) and microwave cooking (900W) on identical samples. Results aim to provide valuable insights for food manufacturers to determine optimal frying conditions for large-scale production of texturized protein products, while developing kinetic models that predict quality changes during the frying process.

6.2.Materials and methods

6.2.1. Materials

Manila tamarind seeds (*Pithecellobium dulce* L) were collected from a local town in Uttar Pradesh, India. Sunflower oil, common salt, wheat gluten and raw jackfruit were purchased from the local market of Tezpur, Assam, India. Jackfruit flour was prepared from the raw jackfruit after drying for 10 h at 60 °C followed by grinding and sieving (mesh number 60). A reference sample was bought from market for comparative study. It contained water, pea protein concentrate, soy protein isolate, dietary fibre, wheat gluten, corn starch, salt, flavours and seasonings.

6.2.2. Chemicals and reagents

Petroleum ether (boiling point 40-60 °C), sodium alginate, calcium chloride and the remaining food-grade and analytical grade substances used in the analysis were all purchased from Octagon Chemicals & Instruments, Zenith India, Guwahati, Assam, India.

6.2.3. Preparation of protein isolates

The extraction of proteins from Manila tamarind seeds followed a modified protocol based on alkaline solubilization and acid precipitation method (López et al., 2018).

Initially, the seeds were processed into fine flour using a traditional stone mill and standardized through a 60-mesh sieve. A homogeneous slurry was prepared by combining the flour with distilled water in a 1:3 ratio under continuous agitation for 60 min. The protein extraction was facilitated by adjusting the slurry's pH to 12.0 using 2 M sodium hydroxide solution, followed by 30 min of continuous stirring. The mixture underwent centrifugation at 7000×g for 20 min to separate the protein-rich supernatant. Protein precipitation was achieved by acidifying the supernatant to pH 4.0 using 1 M hydrochloric acid. The precipitated proteins were collected through centrifugation at 7000×g for 20 min, and the resultant pellet was purified through multiple washing cycles with distilled water, each followed by centrifugation at 7000×g for 20 min. The purified protein pellets were subsequently frozen, lyophilized, and stored for further analysis.

6.2.4. Sample preparation

The preparation for plant-based texturized proteins was based on a previous study **(Objective 1B)**, in which protein isolates (PI) from Manila tamarind seeds were combined at different concentrations with other ingredients like wheat gluten (WG), jackfruit flour (JFF), sodium alginate (SA) and salt to produce the texturized proteins. In this work, the optimized formulation was chosen for further analysis. The detailed preparation of the optimized formulation was as follows: The solid ingredients namely PI, WG, JFF, SA, and salt were mixed with the liquid phase (L), consisting of sunflower oil and water (at a weight ratio of 1:10) to produce a slurry. The resultant slurry was then homogenized using high-pressure homogenizer for 10 min, and poured into cubic silicone molds (3.5 × 3.5 × 3.5 cm). An insulator was placed on top and bottom of the molds, and they were frozen for 8 h at -10 ℃ (1^{st} freezing step). The frozen samples were then taken out and immersed in a 3% $CaCl_2$ solution (w/v), and allowed to stabilize at 4 ℃ for 12 h. The resulting gel was once more frozen in the same way as in the first step, for 8 h at -10 ℃ (2^{nd} freezing step). All the samples were kept at 4 ℃ until examination.

6.2.5. Experimental design for frying

Experiments were based on a two-factor factorial design **(Table 6.1)**. The two factors were frying temperature and frying time. Treatments were applied at 3 levels of frying temperature (150 ℃, 160 ℃, 170 ℃), and 6 levels of frying time (30, 60, 90, 120, 150, 180 s).

Table 6.1: Experimental design based on a two-factor factorial design with 3 levels of frying temperature and 6 levels of frying time

Exp. No.	Frying Temperature (°C)	Frying Time (s)
1	150	30
2	150	60
3	150	90
4	150	120
5	150	150
6	150	180
7	160	30
8	160	60
9	160	90
10	160	120
11	160	150
12	160	180
13	170	30
14	170	60
15	170	90
16	170	120
17	170	150
18	170	180

Data obtained were analyzed using ANOVA for analysis of variance and Duncan's group mean comparison test was used for the mean comparisons of significant treatments. All experiments were carried out in triplicate and statistical tests were performed at 5% level of significance.

6.2.6. Frying of the samples

The samples were diced into cubes of approximately 2 cm×2 cm×1 cm for further frying experiments and their weight was recorded using a weighing scale (CY 224C, Aczet, Mumbai, India). A deep-fat fryer (JSGW 1205/2, Ambala, India) with a capacity of 4.5 L was used for deep-fat frying (DF). The sample to oil weight ratio was about 1:500. The fresh oil was preheated at 150 ℃ for 1 h and then adjusted to one of the three oil

temperatures used for frying in this study (150 ℃, 160 ℃, 170 ℃). Samples were put in a wire basket in the fryer and then deep-fat fried in preheated sunflower oil. Three samples were fried at each of the frying times: 30, 60, 90, 120, 150, 180 s. The fried samples were removed from the frying oil, cooled at room temperature, weighed and placed in plastic Zip-Lock sample bags, and frozen at -20 ℃ in a freezer prior to further analysis.

6.2.7. Microwave cooking of the samples

A modified methodology of Albert et al. (2009) was employed in a systematic way for the microwave cooking, utilizing a standardized microwave oven operating at a fixed power of 900W. Known amount of previously weighed texturized protein samples were placed in a tray and subjected to microwave treatment for six distinct durations of 30, 60, 90, 120, 150, and 180 s. After the microwave cooking, the samples were taken out, placed in a desiccator for 15 min and then their weight was recorded using an analytical balance.

6.2.8. Proximate composition analysis of texturized protein and reference sample

The proximate composition of the texturized protein and reference samples was thoroughly analyzed using standardized methods from the Association of Official Analytical Chemists (AOAC, 2006). Moisture content (MC) determination (AOAC method 934.01) involved a gravimetric approach where 5 g samples underwent thermal drying in a precision-controlled environment at 105 °C for 6 h using a specialized hot-air oven (Model LT-90D, Labtech Engineering Co., Ltd., Germany) until constant weight was achieved. The weight differential before and after the dehydration process provided accurate moisture percentage data, calculated using equation (6.1):

$$\text{MC (\%)} = \frac{(\text{Initial weight} - \text{Final weight})}{\text{Initial weight}} \times 100 \quad (6.1)$$

For lipid quantification, fat extraction was performed using the Soxhlet method (AOAC method 920.39), which employed a continuous solvent extraction system (Soxtec® Avanti 2050 Auto System, Foss Tecator AB, Sweden) with petroleum ether (boiling point 40-60 °C, analytical grade, Merck KGaA, Germany) as the extraction solvent. Samples (2 g) were extracted for 6 h, followed by solvent evaporation and drying of fat

residue at 105 °C for 1 h before weighing. Protein content was determined via the Kjeldahl method (AOAC method 981.10), which quantified nitrogen content using an automated analytical system (Kjeltec® 2300 Analyzer Unit, Foss Tecator AB, Sweden). This technique involved sample digestion (1g) with concentrated sulfuric acid (H_2SO_4) and catalyst mixture (K_2SO_4:$CuSO_4$ = 10:1) at 420 °C for 2 h, followed by distillation with 40% NaOH and titration with standardized 0.1N HCl to determine total nitrogen, which was then converted to protein content using the conversion factor of 6.25. The mineral component was assessed through ash content determination method (AOAC method 942.05) which involved complete incineration of organic matter in pre-weighed crucibles containing 2g samples at 550±10 ℃ for 8 h in a muffle furnace (Thermolyne F6010, Thermo Scientific, USA), leaving only inorganic mineral residues for quantification. For crude fiber analysis, 0.5 g samples were processed in a Fiber Analyzer using sequential H_2SO_4 and NaOH treatments. The final crude fiber content was calculated based on the weight difference after the charred samples were ashed at 550±15 °C for 6 h. All analyses were performed in triplicate.

6.2.9. Moisture content analysis

The moisture content of the fried samples was determined using the AOAC (2006) standard method as discussed in section **6.2.8** using equation 6.1.

6.2.10. Fat content analysis

The dried samples from the earlier analysis were ground using a mortar-pestle. The crude fat content was determined using the Soxhlet extraction method (AOAC, 2006). Clean extraction thimbles were dried in a hot-air oven at 105 °C for 1 h and cooled in a desiccator before being weighed (W_1). The ground samples were then weighed (2 g) (W_2) and placed in the extraction thimble. The thimble was plugged with fat-free cotton wool and placed in the Soxhlet extractor. Clean extraction flasks were dried at 105 °C for 1 h, cooled in a desiccator, and weighed accurately (W_3). The flasks were then filled with approximately 150 mL of petroleum ether (boiling point 40-60 °C). The extraction was carried out at 80-140 °C for 2 h. After extraction, the solvent was recovered, and the extraction flask containing the extracted fat was dried in a hot-air oven at 105 °C for 1 h. The flask was cooled in a desiccator and weighed (W_4). The drying and weighing process was repeated until constant weight was achieved. The crude fat content was

calculated using the following equation (6.2):

$$\text{Crude fat content (\%)} = \frac{W_4 - W_3}{W_2 - W_1} \times 100 \quad (6.2)$$

Where, W_1 is weight of empty thimble (g), W_2 is weight of thimble + sample (g), W_3 is weight of empty extraction flask (g), and W_4 is weight of extraction flask + extracted fat (g).

6.2.11. Kinetic modelling of mass transfer: Diffusion coefficient and activation energy calculation

To accurately describe transfer phenomena, appropriate models should be selected based on their underlying assumptions and theoretical foundations. The infinite slab model was selected based on several key criteria such as uniform initial moisture content, negligible shrinkage and thickness changes, stable oil temperature during frying, bilateral mass transfer through both sides of the samples, and that the sample thickness was significantly smaller than other dimensions (Moreira et al., 1997). For modelling of moisture loss, moisture ratio (MR) was calculated for all moisture content data. These new data were fitted to the appropriate exponential model (6.3).

$$MR = \frac{M - M_e}{M_o - M_e} \quad (6.3)$$

where MR is the moisture ratio (dimensionless), M_e is equilibrium moisture content (g/g, d.b.), M_o is initial moisture content (g/g, d.b.), D_{eff} is effective diffusivity (m^2/s), t is time (s), and L is the thickness of sample (m). With assuming M_e is very small, above equation was simplified into equation (6.4).

$$MR = \frac{8}{\pi}\exp(-kt) \quad (6.4)$$

where k is the rate constant (s^{-1}).

The natural logarithm of the moisture ratio (MR) was then calculated and plotted as the negative natural logarithm versus time. The slope of the straight line fitted to this data represented the rate constant of moisture loss. Using equation 6.5, the effective moisture diffusivity (D_{eff}) was then determined from this rate constant.

$$D_{eff} = \frac{4kL^2}{\pi^2} \quad (6.5)$$

The temperature dependency of the effective diffusivity coefficient for moisture is shown by the Arrhenius expression (Eq. 6.6). Three frying temperature and their particular effective diffusivity values were fitted to this model.

$$D_{eff} = D_o \exp\left(\frac{E_a}{R \times T}\right) \quad (6.6)$$

where, D_o = effective moisture diffusivity (m^2/s), E_a = activation energy for diffusion (kJ/mol), R= gas constant (8.314×10^{-3} kJ/ mol), T= temperature (K).

For modelling of fat uptake, oil content data were fitted to special model (Eq. 6.7) Krokida et al. (2001) by using MATLAB software. Constant rate (k) and equilibrium fat content (C_o) were obtained for all the samples.

$$F_c = C_o[1 - \exp(-kt)] \quad (6.7)$$

where F_c is the fat content (g/g, d.b.) and C_o is the equilibrium fat content (g/g, d.b.).

To evaluate the quality of the kinetic models, the correlation coefficient (R^2), root-mean-square-error (RMSE), and sum of square error (SSE) were used (Alugwu et al., 2022).

6.2.12. Cooking yield and cooking loss calculation

The cooking yield was computed by measuring the difference in weight of the samples before and after frying using equation (6.8) (Palanisamy et al., 2019).

$$\text{Cooking yield (\%)} = \frac{\text{Mass of cooked sample}}{\text{Mass of raw sample}} \times 100 \quad (6.8)$$

Cooking loss was calculated by using the given equation (6.9):

$$\text{Cooking loss (\%)} = (100 - \%\ \text{Cooking yield}) \quad (6.9)$$

6.2.13. Hardness determination / Texture profile analysis

The textural characteristics of the samples were evaluated using a TAXT Plus Texture Analyzer equipped with a 25 mm diameter flat pressure adaptor through the protocol of Chiang et al. (2019) with a few modifications. Samples were uniformly cut into cubic shapes measuring 1×1×1 cm. A double compression test was conducted using a P/50 probe with a 30 kg load cell, compressing samples to 50% of their original height at 60 mm/min. From the resulting force-time curves, multiple textural attributes were derived: hardness, defined as the peak force during the first compression cycle (measured in g); springiness, calculated as the ratio of sample recovery after the initial compression; cohesiveness, determined as the ratio of work done during the second compression relative to that of the first compression; gumminess, computed as the product of hardness and cohesiveness; and chewiness, calculated as the product of hardness, cohesiveness, and springiness (expressed in g). Each sample underwent duplicate testing to ensure measurement reliability, with the derived parameters collectively providing a comprehensive mechanical characterization of the nuggets' textural properties, which correlate strongly with sensory perception during consumption.

6.2.14. Determination of color properties

Color parameters were quantitatively assessed using a precision colorimeter (Chroma meter CR-210, Minolta, Japan) equipped with illuminate C and calibrated using a standardized white reference plate (L^*=97.83, a^*=-0.43, b^*=+1.98). The instrument employed reflectance spectrophotometry with a defined measuring area of 8 mm diameter to capture surface color characteristics. The Commission Internationale de l'Éclairage (CIE) *Lab** color space model was utilized, where L^* represents lightness (0=black, 100=white), a^* indicates red-green chromaticity ($+a^*$=red, $-a^*$=green), and b^* signifies yellow-blue chromaticity ($+b^*$=yellow, $-b^*$=blue). These multidimensional color parameters provide comprehensive characterization of visual properties. Measurements were taken on the surface of nugget samples in triplicate to ensure representative sampling, with results presented as means and standard deviations to account for natural color variations across the sample surface Additional color metrics including total color difference (ΔE) were calculated from triplicate measurements at different sample locations (Dutta & Sit, 2023).

6.2.15. *In-vitro* protein digestibility (IVPD)

The *in-vitro* protein digestibility was determined using the modified methodology of Flores-Jiménez et al. (2022). The process involved preparing a protein suspension (312.5 mg protein in 10 mL distilled water) maintained at 37 °C and adjusted to pH 8.0. A multi-enzyme solution containing trypsin (2.5 mg) and pancreatin (50 mg) in 50 mL distilled water was introduced to the protein suspension. The pH decline was monitored over 10 min, with the final reading used to calculate the *in-vitro* protein digestibility (Equation 6.10):

$$\text{IVPD (\%)} = [210.464 - 18.103(X_1)] \quad (6.10)$$

Where, X_1 = pH at 10 min.

6.2.16. Morphology using Scanning electron microscopy (SEM)

With minor adjustments, the methodology of Samard & Ryu (2019) was used to analyze the microstructure of the texturized protein. Sample preparation involved cutting specimens into 3 mm × 10 mm pieces, flash-freezing them in liquid nitrogen, and subjecting them to vacuum dehydration at 1×10^{-4} mbar for 4 h at -8 °C using an Emitech K1250 Cryo-SEM system. The prepared samples were gold-coated and examined using a JEOL JSM-6460 LV Cryo-SEM at -180 °C.

6.2.17. Comparison of cooking quality between frying and microwave cooking

Samples of texturized proteins that were subjected to two cooking methods of frying at 160 °C (selected based on kinetics) and microwave cooking at 900W across progressive time intervals (30, 60, 90, 120, 150, and 180 s), were analyzed for appearance, moisture content, cooking quality (cooking yield and cooking loss), texture profile analysis parameters (hardness, springiness), color changes (*L**, *a**, *b** values), and *in-vitro* protein digestibility (IVPD). Comparisons were made on the basis of the mentioned parameters and a co-relation analysis was done to find out the best cooking method out of the two methods studied.

6.2.18. Statistical analysis

Statistical analysis was performed with IMS SPSS Statistics 26 software. All measurements were conducted in triplicate, with results expressed as mean ± standard deviation. Statistical differences between samples were evaluated through one-way analysis of variance (ANOVA), followed by Duncan's multiple range test, with $p<0.05$ considered statistically significant.

6.3.Results and discussion

6.3.1. Proximate composition analysis of freeze texturized protein and reference sample

The chemical composition analysis **(Table 6.2)** revealed that the freeze texturized protein had significantly ($p<0.05$) higher moisture content (73.29%) as compared to the reference sample (52.4%). Moisture content plays a crucial role in meat analogue development as it directly influences the protein-protein and protein-water interactions during texturization, affecting the final product's fibrous structure and bite characteristics. Along with other processing parameters, moisture content significantly impacts various product properties such as texture, color, storage stability, and sensory characteristics (Samard et al., 2021; Ketnawa & Rawdkuen, 2023; Liu et al., 2024).

Table 6.2: Proximate composition analysis of texturized protein and reference material (texturized soy protein)

Parameters	Texturized protein	Reference sample (Texturized soy protein)
Moisture (%)	73.29 ± 0.40^{a}	52.4 ± 0.32^{b}
Fiber (%)	2.16 ± 0.02^{b}	9.5 ± 0.32^{a}
Fat (% d.b.)	14.92 ± 0.12^{a}	3.99 ± 0.18^{b}
Protein (% d.b.)	64.12 ± 0.82^{a}	52.10 ± 0.38^{b}

Values are given as mean ± standard deviation. a, b: Different lowercase superscripts within the same rows indicate statistically significant differences *($p<0.05$)*

The fiber content of the sample was 2.16%, which was significantly ($p<0.05$) lower than the reference sample (9.5%). While this lower fiber content may reduce potential health benefits (Anjum et al., 2011; Arueya et al., 2017), it provides advantages for meat-like

texture development through the formation of smooth, cohesive structures that better mimic muscle fiber organization (Djekic, 2015). The fat content in the sample was significantly ($p<0.05$) higher (14.92%) than the reference sample (3.99%). In meat analogues, fat content is particularly important as it influences both nutritional aspects and sensory characteristics, contributing to moisture retention, juiciness, mouthfeel, and flavor perception, similar to the role of intramuscular fat in conventional meat products (Anjum et al., 2011; Ketnawa & Rawdkuen, 2023). The protein content was notably high at 64.12%, significantly ($p<0.05$) exceeding the reference sample (52.1%), attributed to the use of defatted manila tamarind flour for protein isolate preparation. High protein content is essential in meat analogues as it enables better protein-protein interactions during processing, leading to improved texture formation and enhanced nutritional value. This elevated protein content enhances its potential for various food applications (do-Carmo et al., 2023), with optimization focusing on maintaining desirable properties while achieving high protein levels, crucial for meeting industry demands for plant-based alternatives that can effectively replicate the nutritional and functional properties of conventional meat products (Laugesen et al., 2022).

6.3.2. Appearance of the fried samples

The visual analysis of fried samples reveals complex thermal processing dynamics, with **Figure 6.1** demonstrating pronounced color variations across different frying temperatures. The progressive color changes and physical transformation of the samples can be clearly seen. At time 0 s, all the samples (**Figure 6.1 A, B,** and **C)** displayed a similar light orange-yellow color. As frying progressed through 30, 60, 90, 120, 150, and 180 s, a consistent darkening pattern was observed, with the rate and intensity of browning increasing with higher temperatures. Samples fried at 150 ℃ shown a gradual transition from light to dark brown, whereas 160 ℃ samples demonstrated a slightly faster color development, and 170 ℃ samples exhibited the most rapid darkening, reaching nearly black coloration by 150-180 s. The samples exhibited pronounced structural modifications throughout the frying process, transitioning from their original configuration to more condensed forms with increasingly rough surface textures as frying duration extended. As illustrated in **Figure 6.2**, the visual metamorphosis of reference samples subjected to deep-fat frying at 160 °C demonstrated a clear progression of physical and chemical alterations. Initially, the unfried samples (0 s)

displayed a characteristic light-yellow hue, attributable to their native composition and moisture content. This coloration dramatically evolved during thermal processing, with samples progressively darkening through distinct phases of transformation. During the early frying period (30–90 s), the gradual browning can be attributed to Maillard reactions-non-enzymatic interactions between reducing sugars and amino acids that accelerate at temperatures above 140 °C, producing melanoidins responsible for the characteristic brown pigmentation and desirable flavor compounds (Gertz, 2014).

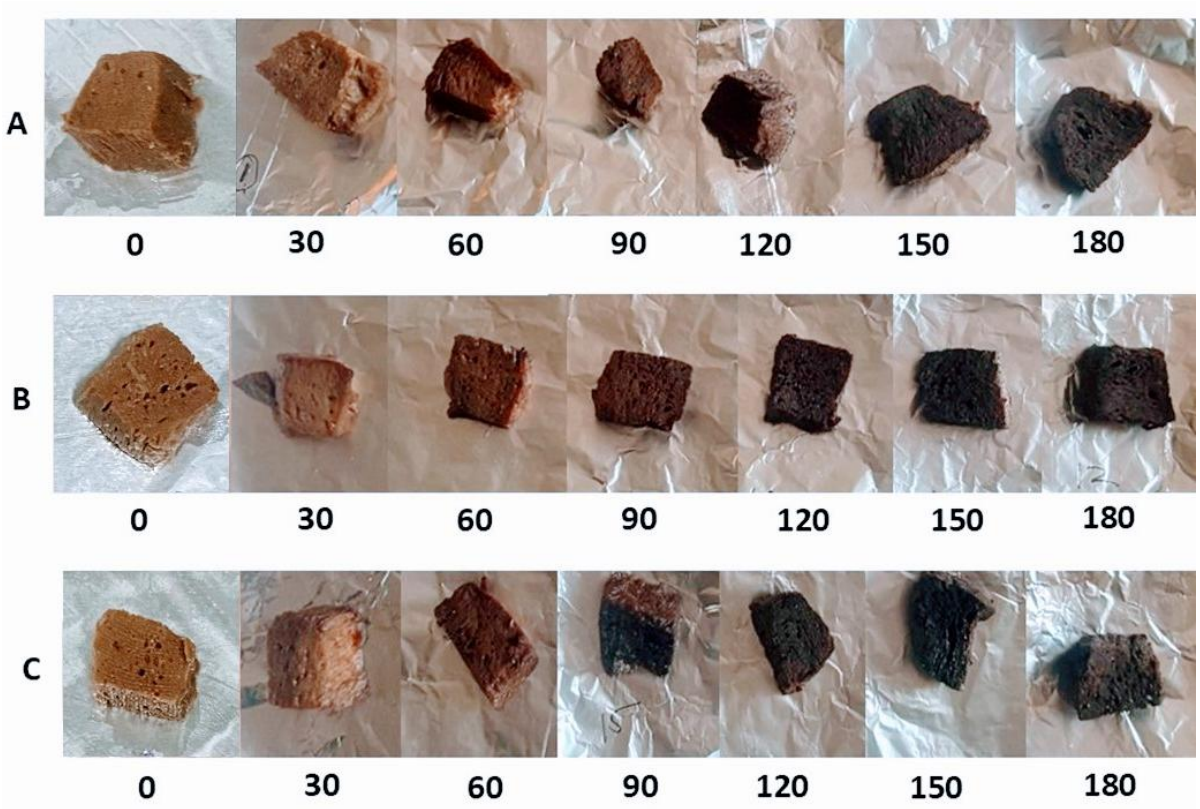

Figure 6.1: The appearance of the of texturized protein samples before frying (0 s) and fried samples after deep-fat frying at different frying times (30, 60, 90, 120, 150, 180 s) and temperatures (A-150 ℃, B-160 ℃, C-170 ℃)

Simultaneously, the initial moisture evaporation creates steam pressure within the food matrix, causing microscopic pore formation that facilitates subsequent oil penetration through capillary action (Kumar et al., 2022). As frying progressed to extended durations (120–180 s), the samples underwent more dramatic physical transformation, becoming significantly darker due to intensified Maillard reaction products and early stages of caramelization of surface carbohydrates, while also developing a notably more compact structure (Krokida et al., 2001). This structural densification results from substantial moisture evacuation from the food matrix (typically reducing moisture content by 30-

50%), protein denaturation causing cellular shrinkage, starch gelatinization followed by retrogradation, and the replacement of water with oil in the created void spaces (Anjum et al., 2011). The rougher surface texture observed at these later stages can be attributed to the formation of a dehydrated crust layer with heterogeneous topography resulting from uneven moisture loss, localized thermal expansion, and the development of microscopic cracks that serve as additional pathways for oil migration into the food matrix (Pedreschi et al., 2005).

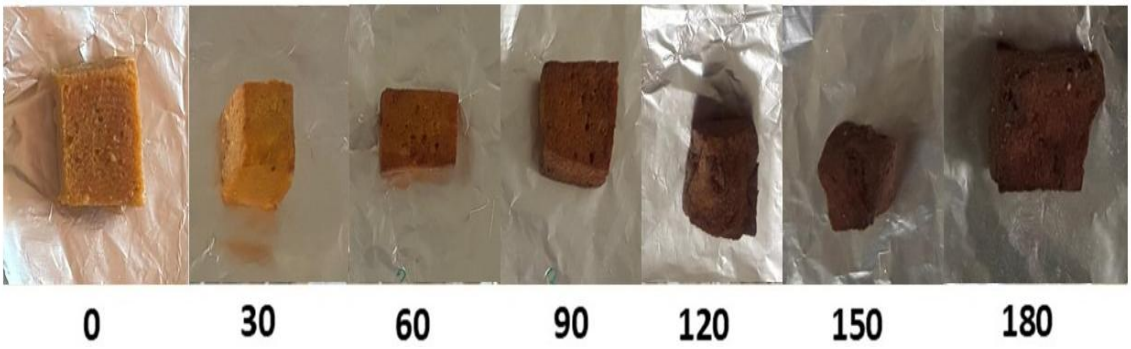

Figure 6.2: The appearance of the reference samples before frying (0 s) and after deep-fat frying at different frying times (30, 60, 90, 120, 150, 180 s) and at a temperature of 160 ℃

When compared, all samples in the **Figure 6.1** and **6.2** exhibited a similar trend of darkening and structural changes with prolonged frying, consistent with Maillard browning reactions and moisture loss during deep-fat frying (Mehta & Swinburn, 2001; Gertz et al., 2014). However, variations in texture, shrinkage, and color intensity are noticeable among the different sample and reference sample images **(Figure 6.1** and **6.2)**, as commonly observed in fried food systems (Miranda & Aguilera, 2006). These differences may indicate variations in composition or initial MC affecting their frying behaviour (Ziaiifar et al., 2008). The changes highlight the impact of frying duration on texture and color development. Color transformation was notably time-dependent, progressively darkening with increased frying duration across all temperature ranges. This visual progression clearly illustrates how both temperature and time affect the development of color and texture in fried texturized proteins. Concurrent with color changes, MC consistently decreased during deep-fat frying, particularly in the latter half of the frying period, a phenomenon substantiated by comparable studies on chicken strips by Vélez-Ruiz et al. (2002) and chicken nuggets by Adedeji et al. (2009), who observed similar moisture reduction patterns at temperatures ranging from 150 to 190 °C.

6.3.3. Moisture content analysis

Table 6.4 presents a comprehensive analysis of moisture content (MC) variations in fried samples across three different temperatures (150 °C, 160 °C, and 170 °C) over a 180 s frying period. Two-way ANOVA **(Table 6.3)** revealed that frying temperature and frying time both had significant impacts on moisture content ($p<0.05$). There was a significant interaction effect ($p<0.05$) since the extent and rate of moisture loss were temperature-dependent. At the initial time point (0 s), all samples contained equivalent moisture content (73.29%). With frying, moisture reduced at all temperatures with different trends. At 150 ℃, moisture fell steadily to 30.48% at 180 s, an indication of a steady drying process. At 160 ℃, moisture fell more precipitously, going as low as 23.11% at 180 s. Remarkably, at 170 ℃, moisture fell quickly initially (52.90% at 30 s), but then exhibited relatively greater retention than 160 ℃ at subsequent times (e.g., 34.50% at 120 s vs. 27.63% at 160 ℃).

Table 6.3: Two-way ANOVA (with interaction) for Moisture Content (% w.b.) and Fat Content (% d.b.) of fried samples

Source of Variation	df	Sum of Squares (SS)	Mean Square (MS)	F-value	p-value
Moisture content					
Frying temperature (A)	2	125.46	62.73	181.23	<0.0001
Frying time (B)	6	5630.84	938.47	2710.58	<0.0001
A × B (Interaction)	12	62.41	5.20	15.04	<0.0001
Error	42	14.51	0.35	–	–
Total	62	5833.22	–	–	–
Fat content					
Frying temperature (A)	2	112.83	56.42	480.32	<0.0001
Frying time (B)	6	958.55	159.76	1360.49	<0.0001
A × B (Interaction)	12	14.72	1.23	10.46	<0.0001
Error	42	4.93	0.12	–	–
Total	62	1091.03	–	–	–

Two-way ANOVA showed that both frying temperature and frying time significantly affected the moisture and fat content of fried samples ($p < 0.001$). Moisture content decreased while fat content increased with longer frying duration and higher temperature. The interaction between the two factors was also significant, suggesting that moisture evaporation and fat absorption were interdependent processes influenced by frying temperature.

Table 6.4: Moisture content (moisture content) values (% w. b.) for fried samples obtained after fat-frying at different temperatures

Time (s)	MC (% w.b.)		
	150 ℃	**160 ℃**	**170 ℃**
0	73.29 ± 0.40^{aA}	73.29 ± 0.40^{aA}	73.29 ± 0.40^{aA}
30	61.26 ± 0.35^{bA}	56.12 ± 0.38^{bB}	52.90 ± 0.33^{bC}
60	48.78 ± 0.42^{cA}	46.20 ± 0.45^{cC}	47.14 ± 0.38^{cB}
90	38.75 ± 0.37^{dB}	40.93 ± 0.32^{dA}	36.28 ± 0.30^{dC}
120	34.89 ± 0.29^{eA}	27.63 ± 0.31^{eB}	34.50 ± 0.27^{eA}
150	31.75 ± 0.33^{fA}	25.21 ± 0.29^{fC}	28.86 ± 0.26^{fB}
180	30.48 ± 0.30^{gA}	23.11 ± 0.28^{gC}	26.85 ± 0.25^{gB}

Values are given as mean ± standard deviation. Means in the same row (i.e., at the same frying time) followed by different uppercase superscript letters (A–C) indicate statistically significant differences between frying temperatures ($p<0.05$). Means in the same column (i.e., at the same temperature) followed by different lowercase superscript letters (a–g) indicate statistically significant differences between frying times ($p<0.05$). Means sharing the same uppercase or lowercase superscript letters are not significantly different ($p>0.05$).

Initially, all samples commenced with a uniform moisture content of 73.29% (wet basis), representing the baseline condition before thermal processing. As frying progressed, a consistent and statistically significant ($p<0.05$) reduction in moisture content was observed across all temperature treatments. Up to 30 s, substantial initial moisture loss was observed, with samples at 150 °C retaining 61.26% moisture, 160 °C samples dropping to 56.12%, and 170 °C samples experiencing the most dramatic reduction to 52.9%. By 60 s, the moisture content stabilized somewhat, with values ranging between 46.2% and 48.78% across temperatures. The 160 °C treatment demonstrated the most pronounced moisture reduction, reaching 23.11% by 180 s, compared to 26.85% at 170 °C and 30.48% at 150 °C. These findings align with research by Ni et al. (2018), who observed similar moisture dynamics during thermal processing of food products, and Moreira et al. (1997), who highlighted the complex interplay between temperature, time, and moisture loss during deep-frying. The differential moisture reduction patterns can be attributed to variations in heat transfer rates, product structure, and thermal degradation mechanisms. The statistically significant differences ($p<0.05$) between temperature

treatments emphasize the critical role of thermal processing parameters in moisture retention and product quality. Notably, the most rapid moisture loss occurred within the first 60 s of frying, suggesting a critical initial phase of thermal moisture expulsion. These results have significant implications for food processing, providing insights into the thermal behaviour of food products and the potential optimization of frying protocols to maintain desired moisture characteristics (Kumar et al., 2022).

6.3.4. Fat content analysis

Table 6.5 reveals the intricate dynamics of fat content accumulation during fat-frying across three temperatures (150 °C, 160 °C, and 170 °C) over 180 s, presenting a detailed examination of oil absorption in deep fat fried texturized protein. Two-way ANOVA **(Table 6.3)** confirmed that time and frying temperature had significant effects on fat uptake ($p<0.05$). The interaction effect was also significant ($p<0.05$) since the extent and rate of fat absorption were different depending on frying temperature. At initial time (0 s), all samples contained equal amounts of fat (14.92%). As frying time increased, fat uptake went up in a progressive manner for all temperatures, but the extent of increment was different. At 150 ℃, fat increased gradually to 29.37% at 180 s, while at 160 ℃ and 170 ℃, the increase was greater, to 32.79% and 35.26% respectively at 180 s. What is remarkable is that fat absorption was highest all times at 170 ℃, intermediate at 160 ℃, and lowest at 150 ℃ at all times after 30 s. Initially, all samples exhibited a uniform fat content of 14.92% on a dry basis. As frying progressed, a consistent and statistically significant ($p<0.05$) increase in fat content was observed across all temperature treatments. The 30 s mark demonstrated rapid fat absorption, with samples at 150 °C reaching 18.24% fat content, 160 °C samples accumulating 21.23%, and 170 °C samples experiencing the most substantial initial fat uptake at 23.48%. As frying progressed to 180 s, fat content continued to rise dramatically, with 150 °C samples reaching 29.37%, and 160 °C samples accumulating 32.79%, and 170 °C samples achieving the highest fat content at 35.26%.

These findings closely align with research by Sanz et al. (2007), who documented similar fat absorption patterns during deep-frying of various food products, and Rimac-Brnčić et al. (2004), who explored the relationship between frying temperature and lipid absorption.

Table 6.5: Fat content values (% d.b.) for fried samples obtained after fat-frying at different temperatures

Time (s)	Fat (% d.b.)		
	150 ℃	**160 ℃**	**170 ℃**
0	14.92 ± 0.12^{gA}	14.92 ± 0.12^{gA}	14.92 ± 0.12^{gA}
30	18.24 ± 0.15^{fC}	21.23 ± 0.18^{fB}	23.48 ± 0.21^{fA}
60	20.70 ± 0.13^{eC}	23.79 ± 0.17^{eB}	25.34 ± 0.19^{eA}
90	22.55 ± 0.11^{dC}	25.42 ± 0.16^{dB}	28.52 ± 0.22^{dA}
120	25.87 ± 0.14^{cC}	28.68 ± 0.19^{cB}	30.83 ± 0.23^{cA}
150	27.11 ± 0.16^{bA}	30.91 ± 0.21^{bB}	32.54 ± 0.25^{bA}
180	29.37 ± 0.18^{aC}	32.79 ± 0.24^{aB}	35.26 ± 0.28^{aA}

Values are given as mean ± standard deviation. Means in the same row (i.e., at the same frying time) followed by different uppercase superscript letters (A–C) indicate statistically significant differences between frying temperatures ($p<0.05$). Means in the same column (i.e., at the same temperature) followed by different lowercase superscript letters (a–g) indicate statistically significant differences between frying times ($p<0.05$). Means sharing the same uppercase or lowercase superscript letters are not significantly different ($p>0.05$).

The progressive fat content increase can be attributed to multiple mechanisms, including product porosity, moisture loss, and thermal-induced structural changes that facilitate lipid penetration. The significant differences between temperature treatments highlight the critical role of thermal processing parameters in determining fat absorption characteristics. Notably, the most rapid fat absorption occurred within the first 60 s of frying, suggesting a critical initial phase of lipid uptake. These results provide crucial insights into food processing dynamics, offering valuable information for understanding and optimizing frying protocols to control fat content and maintain desired product qualities (Kumar et al., 2022).

6.3.5. Kinetic modelling for moisture loss and oil uptake

6.3.5.1.Diffusion coefficient for moisture loss and activation energy calculation

Table 6.6 provides moisture ratio values that were used to evaluate moisture transfer kinetics during the deep-fat frying process of meat analogues at three different

temperatures (150 °C, 160 °C, and 170 °C).

Table 6.6: Moisture ratio values for fried samples obtained after fat-frying at different temperatures

Time (s)	Moisture Ratio (MR)		
	150 ℃	**160 ℃**	**170 ℃**
0	1	1	1
30	0.8358	0.7657	0.7217
60	0.6655	0.6303	0.6431
90	0.5287	0.5584	0.4950
120	0.4760	0.3769	0.4707
150	0.4332	0.3439	0.3937
180	0.4158	0.3153	0.3663

Table 6.7 presents crucial modelling parameters that characterize moisture transfer during the deep-fat frying process of meat analogues at three different temperatures (150 °C, 160 °C, and 170 °C). The first-order kinetic rate constant (k_1) shows the highest value at 160 °C ($6.6\times10^{-3}s^{-1}$), followed by 170 °C ($5.4\times10^{-3}s^{-1}$) and 150 °C ($5.1\times10^{-3}s^{-1}$), with this non-linear trend suggesting that 160 °C might be the optimal temperature for moisture transfer in this specific process. The effective moisture diffusivity (D_{eff}) follows a similar pattern, with the highest value at 160 °C ($2.67\times10^{-7}m^2/s$), indicating enhanced moisture movement at this temperature.

Table 6.7: Modelling parameters for moisture transfer during deep-fat frying (DF) of meat analogues at different temperatures

Samples	k_1 ($\times10^{-3}s^{-1}$)	D_{eff} ($\times10^{-7}$ m^2/s)	E_a (kJ/mol)	R^2	RMSE	SSE ($\times10^{-2}$)
150 ℃	**5.1**	2.06	20.97	0.9488	0.084	3.53
160 ℃	**6.6**	2.67	20.53	0.9716	0.080	3.24
170 ℃	**5.4**	2.18	21.75	0.9573	0.081	3.27

The activation energy (E_a) values ranged from 20.53 to 21.75 kJ/mol, with the highest value observed at 170 °C, suggesting increased energy requirements for moisture transfer

at higher temperatures. The statistical parameters (R^2, RMSE, and SSE) indicate good model fit across all temperatures, with the highest R^2 value of 0.9716 at 160 °C suggesting that this temperature provides the most reliable moisture transfer predictions, while the low RMSE (0.080-0.084) and SSE values (3.24×10^{-2} to 3.53×10^{-2}) across all temperatures confirm the model's accuracy. Ran et al. (2023) reported similar effective moisture diffusivity values ($2.34\times10^{-8}m^2/s$ to $4.95\times10^{-8}m^2/s$) during the deep-fat frying of plant-based protein products at temperatures between 150-170 °C, while research by Manjunatha et al. (2019) found activation energy values ranging from 11.45 and 32.82 kJ/mol for moisture transfer and oil uptake in green peas during thermal processing, aligning with our findings. Additionally, Castro-López et al. (2023) observed optimal moisture transfer at 170 °C during deep-fat frying of chicken nuggets, with diffusion coefficients ranging from 1.46 to 5.2×10^{-7} m^2/s and a study by Costa & Oliveira (1999) demonstrated that the moisture diffusion coefficients during frying typically fall within the range of 2.78×10^{-9} m^2/s to 6.93×10^{-9} m^2/s at temperatures between 140-180 °C.

6.3.5.2.Kinetics of oil uptake

The experimental data presented in **Table 6.8** demonstrates the dynamic behaviour of oil uptake kinetics during deep-fat frying of meat analogues across three temperature points (150 °C, 160 °C, and 170 °C). Analysis reveals that the First-order rate constant (k_2) exhibited a non-monotonic temperature dependence, peaking at 160 °C with a value of 1.202 s^{-1}, while lower values were observed at both 150 °C (0.6853 s^{-1}) and 170 °C (0.4226 s^{-1}). This behaviour suggests an optimal processing window around 160°C for controlling oil uptake kinetics.

Table 6.8: Modelling parameters for oil uptake during deep-fat frying (DF) of meat analogues at different temperatures

Samples	k_2 (s^{-1})	O_{eq} (g/g, d.b.)	R^2	RMSE	SSE
150 °C	0.685	15.60	0.9533	1.624	10.54
160 °C	1.202	17.26	0.9878	0.696	1.94
170 °C	0.422	21.06	0.9563	1.738	12.08

Investigation of the equilibrium oil content (O_{eq}) revealed a direct correlation with temperature, showing a progressive increase from 15.6 (g/g, d.b.) at 150 °C to 17.26 (g/g, d.b.) at 160 °C, ultimately reaching 21.06 (g/g, d.b.) at 170 °C. This trend indicates

enhanced oil absorption capacity of the meat analogue matrix at elevated temperatures, possibly due to structural modifications and increased porosity as a result of high moisture loss at higher temperatures. The kinetic modelling data **(Table 6.9)** reveals complex heat transfer behaviour during deep-fat frying of meat analogues across different temperatures (150, 160 and 170 °C). The first-order rate constant (k_3) shows a non-linear relationship with temperature, ranging from 4.6-5.1×10^{-3} s^{-1}, which aligns with findings by Li et al. (2024) on non-linear thermal degradation in protein-based systems. The thermal diffusivity (α) values decreased from 5.167×10^{-8} m^2/s at 150 °C to 4.747×10^{-8} m^2/s at 160 °C, suggesting reduced heat transfer efficiency at higher temperatures, possibly due to crust formation (Lumanlan et al., 2020).

The reliability of the model was demonstrated through R^2 values exceeding 0.92, though accuracy decreased slightly at higher temperatures as evidenced by increasing RMSE and SSE values, consistent regarding model precision in high-temperature frying processes (Wang et al., 2019).

Table 6.9: Kinetic modeling for heat transfer during deep-fat frying (DF) of meat analogues at different temperatures

Samples	k_3 (×10^{-3} s^{-1})	α (×10^{-8} m^2/s)	R^2	RMSE	SSE (×10^{-2})
150 °C	5.1	5.167	0.9788	0.065	1.6
160 °C	4.6	4.747	0.9527	0.089	3.1
170 °C	4.8	4.953	0.9219	0.121	5.8

Statistical validation of the model demonstrated robust performance across the temperature ranges studied. The model achieved its highest accuracy at 160 °C, as shown by an R^2 value of 0.9878, complemented by the lowest RMSE (0.6963) and SSE (1.939) values. These statistical indicators suggest superior model reliability at 160 °C compared to both 150 °C and 170 °C. Moyano & Pedreschi (2006) documented comparable oil uptake kinetics in plant-based proteins, reporting k_2 values between 0.05-0.58 s^{-1} within the temperature range of 150 and 180 °C. Ang & Miller (1991) observed similar oil content ranges (up to 25.3%) in chicken when deep-fat fried at higher temperatures, confirming the temperature dependent absorption behaviour. Oladejo et al. (2017) identified optimal oil uptake kinetics at 130-170 °C in fried sweet potato, with k_2 values approaching 1.02 min^{-1}.

6.3.6. Cooking yield and cooking loss

The comprehensive analysis presented in **Table 6.11, Table 6.12** and **Table 6.13** reveals the intricate dynamics of cooking yield (CY) and cooking loss (CL) during fat-frying at three distinct temperatures (150 °C, 160 °C, and 170 °C) for sample and at 160 °C for the reference sample over a 180 s duration. From **Table 6.11** & **6.12**, it could be seen that initially (at 0 s), all samples uniformly started with 100% cooking yield and 0% cooking loss, representing the baseline condition before thermal processing. Two-way ANOVA **(Table 6.10)** showed that both frying time and frying temperature significantly influenced CY and CL ($p<0.05$), and in both instances, a significant interaction effect was noted ($p<0.05$).

Table 6.10: Two-way ANOVA (with interaction) for Cooking Yield (CY %) and Cooking Loss (CL %) of fried samples

Source of Variation	df	Sum of Squares (SS)	Mean Square (MS)	F-value	p-value
Cooking Yield					
Frying temperature (A)	2	420.86	210.43	152.17	<0.0001
Frying time (B)	6	13735.62	2289.27	1654.93	<0.0001
A × B (Interaction)	12	108.42	9.04	6.53	<0.0001
Error	42	58.03	1.38	–	–
Total	62	14322.93	–	–	–
Cooking Loss					
Frying temperature (A)	2	486.27	243.13	178.55	<0.0001
Frying time (B)	6	13956.47	2326.08	1708.64	<0.0001
A × B (Interaction)	12	114.15	9.51	6.98	<0.0001
Error	42	57.21	1.36	–	–
Total	62	14614.10	–	–	–

Two-way ANOVA revealed significant effects ($p < 0.001$) of frying temperature and frying time on both cooking yield and cooking loss. Cooking yield decreased while cooking loss increased with prolonged frying and higher temperatures. The significant interaction ($p < 0.001$) indicates that these effects are interdependent—moisture evaporation and mass transfer during frying are strongly temperature-time dependent. The findings align with the expected thermal diffusion and dehydration phenomena governing product yield and texture during deep-fat frying.

At the starting time point (0 s), all the samples recorded 100% CY and 0% CL. With the

course of frying, CY reduced consistently while CL increased, though the amplitude of these changes differed with temperature. At 150 ℃, CY reduced slowly to 56.55% at 180 s, accompanied by a corresponding CL of 43.45%. At 160 ℃, more pronounced changes were observed, with CY dropping to 55.66% and CL increasing to 44.34% at 180 s. At 170 ℃, the reduction in CY was most remarkable, to 50.97%, while CL was at its highest, at 49.03%, during the same duration.

As frying time progressed, a consistent and statistically significant ($p<0.05$) decline in cooking yield and corresponding increase in cooking loss became evident across all temperature treatments. The 150 °C treatment demonstrated a more gradual reduction, with cooking yield decreasing to 56.55% and cooking loss increasing to 43.45% by 180 s. In contrast, the 170 °C treatment exhibited more aggressive mass reduction, with cooking yield plummeting to 50.97% and cooking loss escalating to 49.03% within the same timeframe.

Table 6.11: Cooking yield (CY) values for fried samples obtained after fat-frying at different temperatures

Time (s)	**CY (%)**		
	150 ℃	**160 ℃**	**170 ℃**
0	100.00^{aA}	100.00^{aA}	100.00^{aA}
30	84.09 ± 0.35^{bA}	79.51 ± 0.38^{bB}	78.72 ± 0.29^{bB}
60	82.46 ± 0.33^{cA}	72.86 ± 0.41^{cB}	68.91 ± 0.36^{cC}
90	69.90 ± 0.28^{dA}	67.29 ± 0.37^{dB}	60.28 ± 0.31^{dC}
120	61.15 ± 0.24^{eA}	58.00 ± 0.33^{eB}	56.01 ± 0.29^{eC}
150	59.25 ± 0.29^{fA}	55.64 ± 0.26^{fB}	52.55 ± 0.25^{fC}
180	56.55 ± 0.31^{gA}	55.66 ± 0.34^{fA}	50.97 ± 0.27^{gB}

Values are given as mean ± standard deviation. Means in the same row (i.e., at the same frying time) followed by different uppercase superscript letters (A–C) indicate statistically significant differences between frying temperatures ($p<0.05$). Means in the same column (i.e., at the same temperature) followed by different lowercase superscript letters (a–g) indicate statistically significant differences between frying times ($p<0.05$). Means sharing the same uppercase or lowercase superscript letters are not significantly different ($p>0.05$).

Table 6.12: Cooking loss (CL) values for fried samples obtained after fat-frying at different temperatures

Time (s)	CL (%)		
	150 ℃	**160 ℃**	**170 ℃**
0	0.00^{gA}	0.00^{fA}	0.00^{gA}
30	15.91 ± 0.35^{fA}	20.49 ± 0.38^{eB}	21.28 ± 0.29^{fB}
60	17.54 ± 0.33^{eA}	27.14 ± 0.41^{dB}	31.09 ± 0.36^{eC}
90	30.10 ± 0.28^{dA}	32.71 ± 0.37^{cB}	39.72 ± 0.31^{dC}
120	38.85 ± 0.24^{cA}	42.00 ± 0.33^{bB}	43.99 ± 0.29^{cB}
150	40.75 ± 0.29^{bA}	44.36 ± 0.26^{aB}	47.45 ± 0.25^{bC}
180	43.45 ± 0.31^{aA}	44.34 ± 0.34^{aA}	49.03 ± 0.27^{aB}

Values are given as mean ± standard deviation. Means in the same row (i.e., at the same frying time) followed by different uppercase superscript letters (A–C) indicate statistically significant differences between frying temperatures ($p<0.05$). Means in the same column (i.e., at the same temperature) followed by different lowercase superscript letters (a–g) indicate statistically significant differences between frying times ($p<0.05$). Means sharing the same uppercase or lowercase superscript letters are not significantly different ($p>0.05$).

Table 6.13: Cooking yield (CY) and cooking loss (CL) values for fried reference samples at 160 ℃

Time (s)	Frying at 160 ℃	
	CY (%)	**CL (%)**
0	100 ± 0.00^{a}	0 ± 0.00^{g}
30	85.51 ± 0.91^{b}	14.49 ± 0.35^{f}
60	77.18 ± 0.31^{c}	22.82 ± 0.42^{c}
90	73.27 ± 0.65^{d}	26.73 ± 0.37^{d}
120	68.42 ± 0.54^{e}	31.58 ± 0.29^{c}
150	64.56 ± 1.38^{f}	35.44 ± 0.33^{b}
180	64.02 ± 0.42^{f}	35.98 ± 0.30^{a}

Values are given as mean ± standard deviation. a, b, c, d, e, f, g: Different lowercase superscripts within the same column indicate statistically significant differences *($p<0.05$)*

The intermediate temperature (160 °C) showcased a pattern between these two extremes,

with cooking yield dropping to 55.66% and cooking loss reaching 44.34% at 180 s. At 160 °C, the sample and reference sample exhibited notably different cooking yield patterns over the 180 s frying period. The experimental sample showed a more rapid initial moisture loss, with cooking yield decreasing to 79.51% at 30 s and 72.86% at 60 s, compared to the reference sample's higher yields of 85.51% and 77.18% at the same time points, respectively ($p<0.05$). By the end of the frying period (180 s), the experimental sample retained significantly less mass with a final cooking yield of 55.66%, while the reference sample maintained a higher yield of 64.02%. This difference in final cooking yield suggests that the experimental sample was more susceptible to moisture loss and structural changes during frying compared to the reference sample (Park & Kim, 2021). These findings corroborated with research by Krokida et al. (2001), who observed similar moisture and mass transfer phenomena during frying of various food products, and the research by Alugwu et al. (2022) demonstrated that higher frying temperatures accelerate moisture expulsion and structural degradation. The progressive decline in cooking yield can be attributed to multiple simultaneous phenomena, including moisture evaporation, lipid absorption, and thermal-induced protein denaturation. The significant differences between temperature treatments underscore the critical role of thermal processing parameters in determining final product characteristics. Notably, the most rapid changes in cooking yield and loss occur within the first 90 s of frying, suggesting a critical initial phase of thermal transformation. These results have substantial implications for food processing, quality control, and nutritional considerations, highlighting the importance of precise temperature management in achieving desired sensory and structural outcomes.

6.3.7. Analysis of texture profile parameters

Table 6.15, Table 6.16 and **Table 6.17** provide a comprehensive analysis of hardness and springiness characteristics for fried samples processed at three different temperatures (150 °C, 160 °C, and 170 °C) over a 180 s duration. Two-way ANOVA **(Table 6.14)** revealed that frying temperature and frying time also significantly affected hardness and springiness ($p<0.05$) with significant interaction effect for both ($p<0.05$). At the starting point (0 s), hardness and springiness were comparable for all treatments (614.9 g and 0.976, respectively). As frying continued, hardness rose strongly, but the magnitude and maximum values varied with temperature. Under 150 ℃, hardness increased consistently

to a high of 1485.49 g at 120 s before dropping to 1211.49 g at 180 s. Under 160 ℃, the highest reading overall was achieved (1908.82 g at 120 s) before a drop, whereas at 170 ℃, the highest reading was achieved earlier (1523.09 g at 90 s) and plummeted subsequently to 1266.31 g at 180 s. Springiness exhibited more muted but temperature-related fluctuations. Whereas initial values were also high (0.976), springiness would fall with frying, particularly at 170 ℃, falling to 0.895 at 180 s. At 150 ℃ and 160 ℃, springiness was relatively higher, varying between 0.918–0.949 at most time points. At the initial point (0 s), all samples exhibited identical baseline properties, with a hardness of 614.9 and springiness of 0.976, representing the unprocessed state.

Table 6.14: Two-way ANOVA (with interaction) for Hardness (g) and Springiness of fried samples

Source of Variation	df	Sum of Squares (SS)	Mean Square (MS)	F-value	*p*-value
Hardness					
Frying temperature (A)	2	1,565,280.23	782,640.12	186.37	<0.0001
Frying time (B)	6	22,834,511.76	3,805,751.96	905.81	<0.0001
A × B (Interaction)	12	161,438.22	13,453.18	3.20	0.0021
Error	42	176,377.49	4,199.46	–	–
Total	62	24,737,607.70	–	–	–
Springiness					
Frying temperature (A)	2	0.0087	0.00435	92.56	<0.0001
Frying time (B)	6	0.0231	0.00385	81.94	<0.0001
A × B (Interaction)	12	0.0015	0.00013	2.80	0.0083
Error	42	0.0019	0.000045	–	–
Total	62	0.0352	–	–	–

Both hardness and springiness were significantly influenced ($p < 0.001$) by frying temperature and time, with notable interactions. Hardness increased to a maximum at 120 s due to surface crusting and internal moisture loss, followed by a slight decline at prolonged frying. In contrast, springiness decreased with temperature and time, indicating a loss of elasticity associated with protein denaturation and dehydration. These textural trends highlight the opposing behaviours of structural rigidity and elasticity as frying progresses.

As frying progressed, significant ($p<0.05$) changes in both hardness and springiness were observed across all temperature treatments. At the 30 s mark, substantial textural modifications were observed, with hardness increasing dramatically: 895.24 at 150 °C, 925.12 at 160 °C, and a notable peak of 1055.62 at 170 °C. Springiness, conversely, demonstrated a slight initial decline across all temperatures, ranging from 0.904 to 0.918. The most pronounced hardness development occurred at 60 s, with values reaching 1139.15 at 150 °C, 1341.43 at 160 °C, and 1436.98 at 170 °C, indicating a clear temperature-dependent effect on product texture.

Table 6.15: Hardness values for fried samples obtained after fat-frying at different temperatures

	Hardness (g)		
Time (s)	**150 ℃**	**160 ℃**	**170 ℃**
0	614.9 ± 15.2^{gA}	614.9 ± 15.2^{gA}	614.9 ± 15.2^{fA}
30	895.24 ± 20.4^{fB}	925.12 ± 18.7^{fB}	1055.62 ± 25.3^{eA}
60	1139.15 ± 22.8^{eC}	1341.43 ± 26.1^{eB}	1436.99 ± 29.4^{cA}
90	1392.89 ± 24.7^{bB}	1576.95 ± 28.9^{dA}	1523.09 ± 30.8^{bA}
120	1485.49 ± 26.4^{aC}	1908.82 ± 35.2^{aA}	1689.45 ± 33.7^{aB}
150	1358.32 ± 23.5^{cC}	1833.91 ± 32.9^{bA}	1444.72 ± 27.8^{cB}
180	1211.49 ± 21.6^{dC}	1676.44 ± 30.1^{cA}	1266.31 ± 25.5^{dB}

Values are given as mean ± standard deviation. Means in the same row (i.e., at the same frying time) followed by different uppercase superscript letters (A–C) indicate statistically significant differences between frying temperatures ($p<0.05$). Means in the same column (i.e., at the same temperature) followed by different lowercase superscript letters (a–g) indicate statistically significant differences between frying times ($p<0.05$). Means sharing the same uppercase or lowercase superscript letters are not significantly different ($p>0.05$).

Interestingly, the hardness progression did not follow a linear trajectory, with peak values observed at different time points for each temperature treatment. The 120 s mark showed maximum hardness values of 1485.49 at 150 °C, 1908.82 at 160 °C, and 1689.45 at 170 °C, followed by a subsequent reduction by 180 s. Springiness demonstrated more subtle variations, maintaining values between 0.894 and 0.977 throughout the frying process. These findings align with research by Xue & Ngadi (2006), who observed similar textural transformations during thermal processing of meat products, and

explored the mechanisms of texture development in heat-treated foods.

Table 6.16: Springiness values for fried samples obtained after fat-frying at different temperatures

	Springiness		
Time (s)	**150 ℃**	**160 ℃**	**170 ℃**
0	0.976 ± 0.003^{aA}	0.976 ± 0.003^{aA}	0.976 ± 0.003^{aA}
30	0.918 ± 0.004^{cA}	0.904 ± 0.005^{eC}	0.910 ± 0.006^{dB}
60	0.949 ± 0.005^{bA}	0.949 ± 0.003^{cA}	0.894 ± 0.004^{eB}
90	0.977 ± 0.004^{aA}	0.961 ± 0.003^{bB}	0.930 ± 0.005^{cC}
120	0.943 ± 0.005^{bA}	0.937 ± 0.004^{dC}	0.940 ± 0.004^{bB}
150	0.932 ± 0.004^{bB}	0.941 ± 0.003^{dA}	0.923 ± 0.005^{cC}
180	0.943 ± 0.004^{bB}	0.949 ± 0.004^{cA}	0.895 ± 0.003^{eC}

Values are given as mean ± standard deviation. Means in the same row (i.e., at the same frying time) followed by different uppercase superscript letters (A–C) indicate statistically significant differences between frying temperatures ($p<0.05$). Means in the same column (i.e., at the same temperature) followed by different lowercase superscript letters (a–g) indicate statistically significant differences between frying times ($p<0.05$). Means sharing the same uppercase or lowercase superscript letters are not significantly different ($p>0.05$).

When comparing the sample with reference sample at 160 °C, both the experimental and reference samples showed increasing hardness values during frying, but with distinct patterns. The experimental sample exhibited a peak hardness of 1908.82g at 120 s, while the reference sample reached a higher maximum of 2057.92g at the same time point. Interestingly, the springiness characteristics differed markedly - the experimental sample maintained relatively stable springiness (ranging from 0.904 to 0.961) throughout the frying period, while the reference sample showed a substantial decline in springiness from 0.985 to 0.753 (Kim et al., 2024). These differences suggest that while the reference sample developed a harder crust, it experienced more significant textural degradation in terms of elasticity, possibly due to differences in protein structure and moisture retention mechanisms (Xia et al., 2023). The observed variations can be attributed to complex physicochemical changes, including protein denaturation, moisture loss, and structural rearrangement during thermal processing.

Table 6.17: Hardness and springiness values for fried reference samples at 160 ℃

Time (s)	Frying at 160 ℃	
	Hardness (g)	**Springiness**
0	672.52±12.1^{g}	0.985±0.008^{a}
30	939.93±9.3^{f}	0.892±0.005^{d}
60	1465.47±14.2^{e}	0.95±0.006^{b}
90	1640.09±24.6^{d}	0.915±0.009^{c}
120	2057.92±19.8^{a}	0.848±0.004^{e}
150	1928.19±21.3^{b}	0.767±0.01^{f}
180	1763.09±16.2^{c}	0.753±0.002^{g}

Values are given as mean ± standard deviation. a, b, c, d, e, f, g: Different lowercase letter superscripts within the same columns, indicate statistically significant differences *($p<0.05$)*

The statistically significant differences between temperature treatments underscore the critical role of thermal parameters in determining final product texture. These results provide valuable insights into the intricate relationship between frying conditions and food material properties, offering crucial information for optimizing processing protocols and predicting product quality.

6.3.8. Determination of color properties

Figure 6.3, Figure 6.4 and **Table 6.18** provide a comprehensive analysis of color transformation during fat-frying across three temperatures (150 °C, 160 °C, and 170 °C) over 180 s, examining changes in lightness (L^*), redness (a^*), and yellowness (b^*) values. Initially, all samples exhibited identical color characteristics: L^* of 51.01, a^* of 7.6, and b^* of 12.1, representing the baseline condition. As frying progressed, statistically significant ($p<0.05$) color modifications occurred across all temperature treatments. Lightness (L^*) demonstrated a consistent decline, indicating progressive darkening: at 180 s, samples reached 38.3 at 150 °C, 33.23 at 160 °C, and 32.25 at 170 °C, suggesting more intense thermal degradation at higher temperatures. Redness (a^*) values showed a gradual reduction from initial 7.6 to final ranges between 1.03 and 2.23, indicating diminishing red hues during thermal processing.

Table 6.18: Colour values (*L**, *a**, *b**) for reference samples obtained after fat-frying at 160 ℃

Time (s)	Colour parameters		
	L*	***a****	***b****
0	52.48±0.24[a]	18.98±0.24[a]	26.4±0.24[a]
30	47.56±0.32[b]	15.58±0.28[b]	15.95±0.25[b]
60	45.73±0.29[b]	12.11±0.26[c]	8.39±0.27[c]
90	42.73±0.26[c]	10.93±0.22[d]	6.62±0.25[d]
120	40.5±0.21[d]	8.83±0.20[e]	5.7±0.23[e]
150	39.82±0.18[e]	7.54±0.17[f]	4.93±0.22[f]
180	38.83±0.15[f]	7.29±0.14[f]	4.01±0.16[g]

*L**: Lightness; *a**: Redness; *b**: Yellowness. Values are given as mean ± standard deviation. a, b, c, d, e, f, g: Different lowercase letter superscripts within the same columns, indicate statistically significant differences *($p<0.05$)*

Yellowness (*b**) exhibited the most dramatic transformation, declining from 12.1 to near-zero or negative values by 180 s, with particularly pronounced changes at 160 °C and 170 °C. The total color change (ΔE) **(Figure 6.4)** demonstrates a progressive increase across all frying temperatures (150 °C, 160 °C, and 170 °C) over the 180 s frying period. As observed in **Figure 6.4**, higher frying temperatures resulted in more rapid color development, with samples at 170 °C showing the steepest increase in ΔE values during the initial 60 s, followed by those at 160 °C and 150 °C. After 90 s, the rate of color change began to plateau across all temperatures, indicating the stabilization of Maillard reaction products and other color-forming compounds (Sivaranjani et al., 2024). The color parameters of the reference samples **(Table 6.18)** during deep-fat frying at 160 °C exhibited consistent darkening and color intensity reduction over time. The lightness (*L**) value decreased significantly from 52.48 to 38.83, indicating progressive darkening of the surface. Similarly, both redness (*a**) and yellowness (*b**) values showed substantial reductions, with *a** decreasing from 18.98 to 7.29 and *b** showing the most dramatic decline from 26.4 to 4.01.

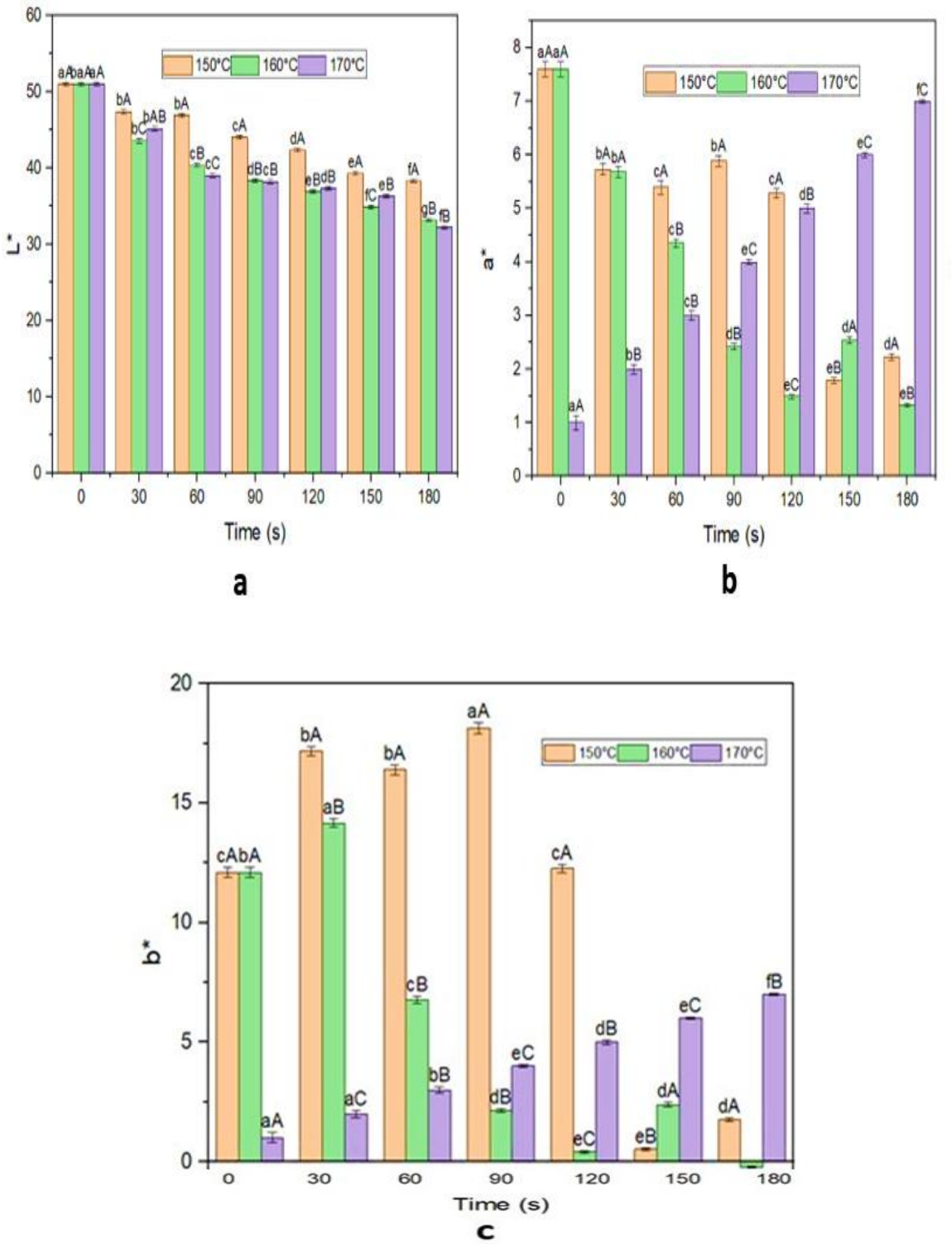

Figure 6.3: The surface color variations (a: *L**, b: *a**, c: *b**) of the samples during deep-fat frying at different temperatures (150, 160 & 170 ℃) and time (0, 30, 60, 90, 120, 150, 180 s)

(Values are given as mean ± standard deviation (SD). a, b, c, d, e, f, g, A, B, C: Different lowercase and uppercase letter superscripts indicate statistically significant differences ($p<0.05$))

This trend suggests the formation of brown compounds through Maillard reactions and potential caramelization during the frying process, with the most pronounced changes occurring within the first 60 s of frying. These findings closely correspond with research by Pedreschi et al. (2005), who documented similar color evolution during potato frying, and Pedreschi & Zúñiga (2009), who explored chromatic modifications in thermal processing. Mesías & Delgado-Andrade (2017) further substantiated these observations, highlighting the complex Maillard reaction mechanisms responsible for color development. Mondal & Dash (2017) demonstrated that temperature and duration significantly influence color kinetics, consistent with the observed variations in this study. The statistically significant differences between temperature treatments emphasize the critical role of thermal parameters in determining final product color characteristics, providing valuable insights into the intricate relationship between frying conditions and visual properties.

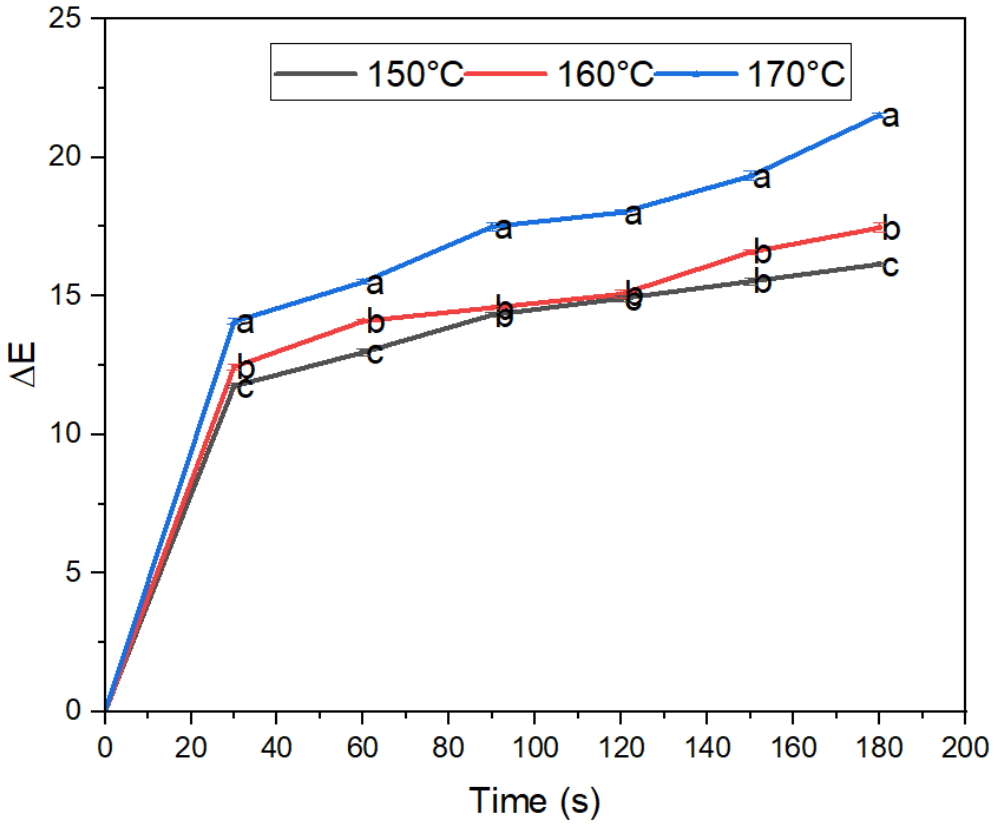

Figure 6.4: The total color change ΔE of the samples during deep-fat frying at different temperatures (150, 160 &170 ℃) and time (0, 30, 60, 90, 120, 150, 180 s)

Values are given as mean ± standard deviation (SD). Different lowercase letter superscripts indicate statistically significant differences ($p<0.05$)

6.3.9. *In-vitro* protein digestibility (IVPD)

Table 6.19 and **Table 6.20** present the *in-vitro* protein digestibility (IVPD) during fat-frying across three temperatures (150 °C, 160 °C, and 170 °C) for sample and reference sample, respectively, for a time period of up to 180 s. The protein digestibility showcased significant ($p<0.05$) improvement across all the temperature ranges. At the 30 s interval, IVPD values escalated to 71.28% (150 °C), 72.86% (160 °C), and 74.57% (170 °C), indicating temperature-induced protein structural transformations. Upon reaching 180 s, digestibility peaked at 77.58% (150 °C), 81.02% (160 °C), and an exceptional 84.98% (170 °C), highlighting a direct correlation between elevated temperatures and increased protein digestibility. When comparing the sample with the reference sample **(Table 6.20)**, the *in-vitro* protein digestibility (IVPD) data reveals interesting patterns across different frying temperatures and time points. At 160 °C, the experimental sample showed a steady increase in IVPD from an initial value of 64.33% to 81.02% after 180 s, while the reference sample exhibited higher overall digestibility, starting at 68.12% and reaching 85.78% under the same conditions (Cao et al., 2024). This enhanced digestibility in both samples suggests that thermal processing positively impacts protein accessibility, likely due to protein denaturation and structural changes that expose more peptide bonds to enzymatic hydrolysis.

Table 6.19: *In-vitro* protein digestibility (IVPD) values for fried samples obtained after fat-frying at different temperatures

Time (s)	IVPD (%)		
	150 ℃	**160 ℃**	**170 ℃**
0	64.33 ± 0.30^{gA}	64.33 ± 0.30^{gA}	64.33 ± 0.30^{gA}
30	71.28 ± 0.55^{fC}	72.86 ± 0.42^{fB}	74.57 ± 0.48^{fA}
60	73.15 ± 0.50^{eC}	75.27 ± 0.47^{eB}	76.44 ± 0.42^{eA}
90	74.06 ± 0.48^{dC}	76.71 ± 0.50^{dB}	77.90 ± 0.54^{dA}
120	75.35 ± 0.62^{cC}	78.17 ± 0.45^{cB}	79.86 ± 0.56^{cA}
150	76.02 ± 0.55^{bC}	79.39 ± 0.58^{bB}	81.93 ± 0.63^{bA}
180	77.58 ± 0.49^{aC}	81.02 ± 0.52^{aB}	84.98 ± 0.58^{aA}

Values are given as mean ± standard deviation. a, b, c, d, e, f, g, A, B, C: Different lowercase and uppercase letter superscripts within the same column and rows, respectively, indicate statistically significant differences *($p<0.05$)*

The higher IVPD values in the reference sample might be attributed to differences in protein composition or matrix structure that facilitate better enzyme access during digestion (Lee et al., 2023). These findings resonate with research by Giami et al. (2001), who documented protein digestibility enhancements during thermal processing, and Gani et al. (2012), who explored protein denaturation mechanisms. Morales et al. (2015) further elucidated the structural changes contributing to increased protein accessibility, while Bhat et al. (2021) highlighted the role of thermal treatments in protein functionality. The observed variations can be attributed to protein structural unfolding, reduced steric hindrance, and increased enzymatic accessibility during heat treatment. The statistically significant differences between temperature treatments underscore the critical role of thermal parameters in modifying protein digestibility, providing valuable insights into the complex interactions between heat processing and protein nutritional characteristics.

Table 6.20: *In-vitro* protein digestibility (IVPD) values for fried reference samples obtained after fat-frying at 160 ℃

Time (s)	IVPD (%)
0	68.12 ± 0.82^{g}
30	74.68 ± 0.93^{f}
60	77.35 ± 1.02^{e}
90	80.05 ± 0.86^{d}
120	82.92 ± 0.94^{c}
150	84.16 ± 0.90^{b}
180	85.78 ± 1.06^{a}

Values are given as mean ± standard deviation. a, b, c, d, e, f, g: Different lowercase letter superscripts within the same column indicate statistically significant differences *($p<0.05$)*

6.3.10. Morphology using scanning electron microscopy (SEM)

The microstructural changes in sample and reference sample before and after frying at 160 ℃ for 90 s is shown in **Figure 6.5** and **6.6**. The SEM images of the samples before frying in both the figures depict relatively uniform, tight, homogeneous, cohesive microstructures, while the images of the fried samples reveal increased heterogeneity,

with the formation of irregularly shaped pockets, fragmentation, and the emergence of various-sized voids and discontinuities. Comparing the two images **(Figure 6.5 & 6.6)**, the microstructural changes appear similar, suggesting the frying process at 160 ℃ for 90 s had a comparable impact on both the sample and the reference material. The disruption of the internal structure likely affects the quality, texture, and nutritional properties of the fried products in both cases (Saguy & Dana, 2003; Nikmaram et al., 2017; Yang et al., 2019). **Figure 6.5** and **6.6** presents 8 micrographs showing microstructural changes in samples before **(Figure 6.5 a** and **6.6 a)** and after **(Figure 6.5 b** and **6.6 b)** frying at 160 °C for 90 s. The images **(a: i, ii, iii, iv)** show uniform, cohesive microstructures. The images **(b: i, ii, iii, iv)** reveal more porous, disrupted structures with voids and discontinuities, indicating frying caused breakdown of the internal organization. The changes include formation of irregularly shaped pockets, fragmentation, and increased heterogeneity and porosity. These microstructural alterations likely impact the quality, texture, and nutritional properties of the fried products.

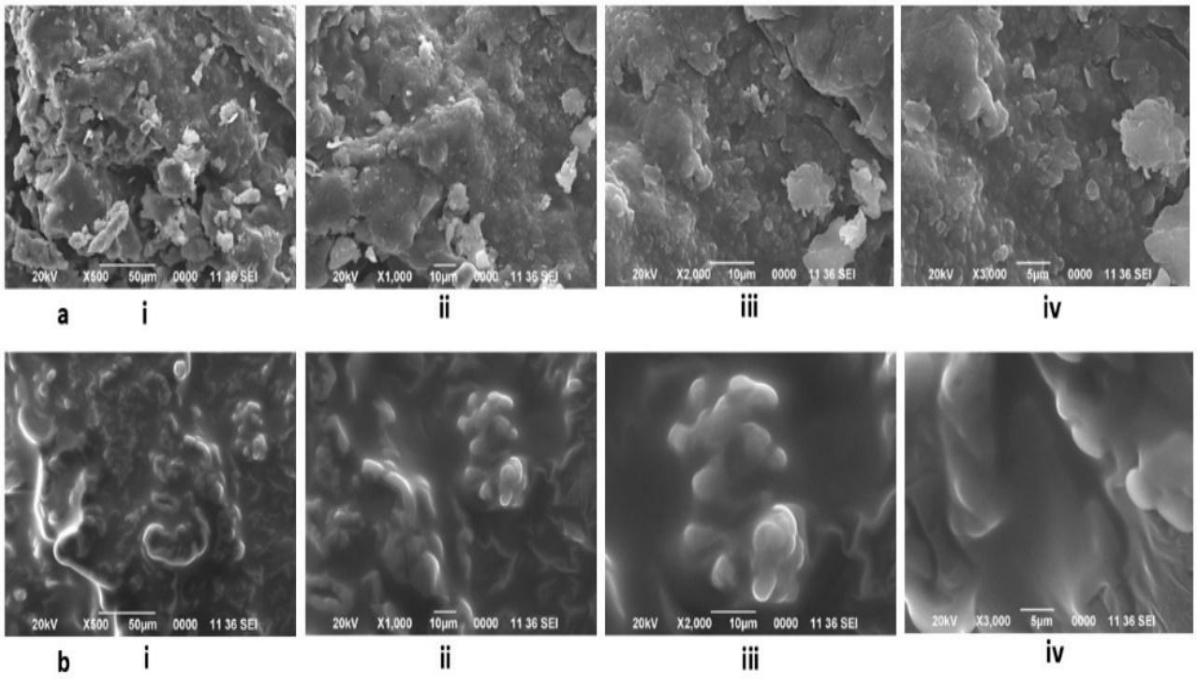

Figure 6.5: The microstructural changes of samples before (a) and after (b) frying at 160 ℃ for 90 s

(at different magnifications (i: 500X, ii: 1000X, iii: 2000X, and iv: 3000X)

These microstructural changes observed in the samples after frying at 160 °C for 90 s can be attributed to several factors. The high temperature and prolonged exposure to frying likely caused physical and chemical transformations within the sample, leading to the breakdown of its internal structure. For example, the formation of voids and pockets may be the result of the rapid expansion and evaporation of moisture within the sample during the frying process (Saguy & Dana, 2003). Additionally, the disruption of the sample's cohesiveness and the creation of a more heterogeneous microstructure could be linked to the degradation of certain components or the rearrangement of the sample's constituents due to the thermal stresses imposed by frying Yang et al. (2019).

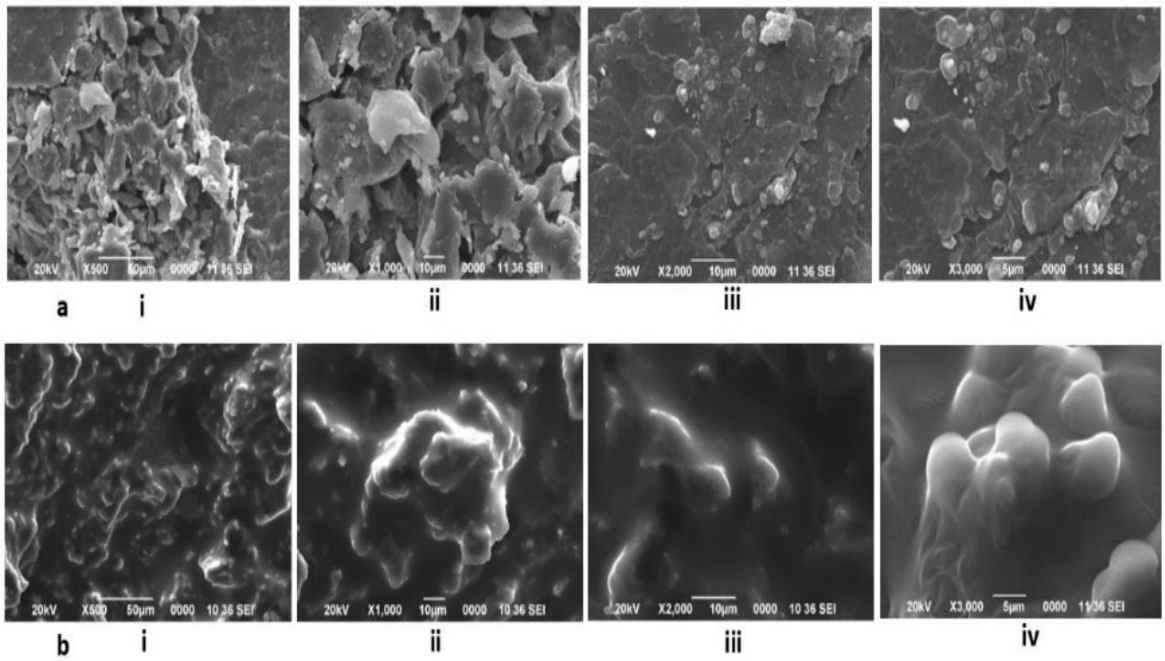

Figure 6.6: The microstructural changes of reference samples before (a) and after (b) frying at 160 °C for 90 s

(at different magnifications (i: 500X, ii: 1000X, iii: 2000X, and iv: 3000X)

The observed microstructural changes have important implications for the quality and properties of the fried products. The formation of voids and discontinuities in the microstructure can affect the texture, mouthfeel, and overall sensory attributes of the fried food, potentially leading to undesirable characteristics such as increased hardness, brittleness, or a less-than-optimal mouthfeel (Saguy & Dana, 2003; Yang et al., 2019). Additionally, the disruption of the microstructure may also impact the nutritional and functional properties of the fried food, as the changes in the internal structure can

influence the accessibility and bioavailability of certain nutrients or compounds (Nikmaram et al., 2017).

6.3.11. Correlation analysis

The correlation heatmap reveals complex relationships between mass transfer, heat transfer, and product quality parameters during deep-fat frying processes **(Figure 6.7)**. The analysis shows that k_1 (First-order rate constant) exhibits strong positive correlations with multiple parameters, notably with D_{eff} (r = 1.00) and hardness (r = 0.95), while showing strong negative correlations with k_3 (r = -0.90) and α (r = -0.94). These relationships indicate that faster initial moisture loss rates (k_1: 3.2-5.8 × 10^{-3} s^{-1}) are associated with higher effective moisture diffusivity and increased product hardness, but inversely related to thermal diffusivity.

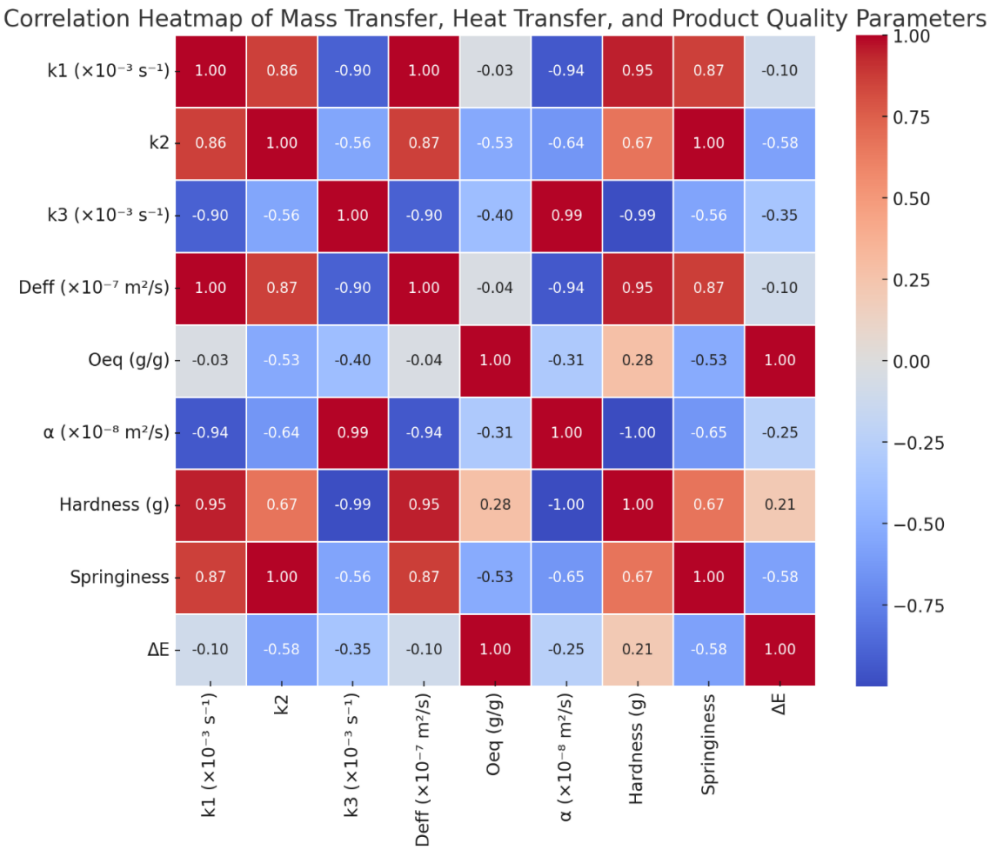

Figure 6.7: Correlation heatmap showing the relationships between mass transfer parameters (k_1, k_2, k_3), heat transfer parameters (D_{eff}, α), and product quality attributes (O_{eq}, Hardness, Springiness, and ΔE)

The effective moisture diffusivity (D_{eff} - 2.8 to 4.5 × 10^{-7} m^2/s) demonstrates identical correlation patterns to k_1, with strong positive correlations with hardness (r = 0.95) and springiness (r = 0.87), and negative correlations with k_3 (r = -0.90) and α (r = -0.94) suggesting the interconnected nature of moisture movement and textural development during frying. The thermal diffusivity (α- 4.2 to 5.9 × 10^{-8} m^2/s) shows a nearly perfect positive correlation with k_3 (r = 0.99, k_3: 3.8-6.2 × 10^{-3} s^{-1}) and strong negative correlations with hardness (r = -1.00) and k_1 (r = -0.94), suggesting that higher thermal diffusivity values are associated with slower moisture loss rates but faster heat transfer rates as explained by Islam (2023).

The equilibrium oil content (O_{eq}) exhibited relatively weak correlations with most parameters, with the strongest being negative correlations with k_2 and springiness, while showing a perfect positive correlation with color change (ΔE). These findings were in agreement with findings of Wang et al. (2024) who reported that oil uptake mechanisms were more influenced by surface phenomena than internal heat and mass transfer. The textural parameters (hardness and springiness) show strong correlations with mass transfer parameters but inverse relationships with thermal parameters, with hardness particularly showing strong correlations with k_1 and k_3, while springiness perfectly correlates with k_2. This was in agreement with the findings of Dana & Saguy (2006), who reported that who reported that oil uptake mechanisms were more influenced by surface phenomena than internal heat and mass transfer and showed inverse relationships with thermal parameters due to the formation of a dehydrated crust layer that significantly affects product hardness and springiness. The textural parameters (hardness and springiness) show strong correlations with mass transfer parameters but inverse relationships with thermal parameters, with hardness particularly showing strong correlations with k_1 and k_3, while springiness perfectly correlates with k_2. Recent work by Liu et al. (2024) revealed a fascinating relationship between texture formation and moisture dynamics during frying. Their research demonstrates that as moisture escapes, it leads to crust development, which fundamentally shapes both hardness and springiness characteristics of the product. When examining color transformations, our data shows limited correlation with most variables, though several striking connections were found with oil absorption (r = 1.00) and modest negative associations with both k_2 and springiness (r = -0.58). This pattern suggests that color development primarily stems from surface-level changes and chemical interactions rather than deeper thermal and

mass movement processes. Building on this understanding, Delgado-Andrade et al. (2010) conducted experiments at elevated temperatures that shed light on the browning mechanism. Their work revealed that surface color development depends mainly on Maillard reaction progression and surface heat transfer through oil, while internal moisture movement plays only a minor role. Their findings showed that color intensity (ΔE) directly tracks with surface oil levels (ranging from 8.5% to 16.2%) and cooking temperature. However, they found minimal relationship between color development and internal heat transfer metrics, reinforcing that surface chemistry, rather than internal thermal dynamics, governs color formation (Delgado-Andrade et al., 2010).

6.3.12. Comparison of cooking quality between frying and microwave cooking

6.3.12.1. Appearance of the cooked samples

The image **(Figure 6.8)** presents a comparative visual representation of texturized protein samples subjected to two distinct cooking methods-fat-frying **(Figure 6.8a)** and microwave (MW) cooking **(Figure 6.8b)** over different cooking durations (30, 60, 90, 120, 150, and 180 s), illustrating progressive changes in texture, color, and structural integrity. Initially, the raw samples exhibited a uniform light brown color with a porous and spongy texture, indicating their hydrated state before thermal processing. As cooking progressed in both methods, distinct transformations emerged. In fat-frying **(Figure 6.8a)**, the samples underwent noticeable darkening, with color shifting from light brown at 30 s to an almost black, charred appearance at 180 s. This was likely due to the Maillard reaction and caramelization, which intensified at high temperatures, particularly in the presence of oil (Ahmed & Mohammed, 2023). The textural structure also appeared to shrink and compact over time, potentially due to moisture loss and surface hardening from direct oil contact. By 120 s and beyond, the samples exhibited significant surface browning, indicative of protein denaturation and possible formation of a crust-like layer that may have limited further moisture evaporation from the core (Le et al., 2023). Conversely, MW cooked samples **(Figure 6.8b)** underwent a different transformation, retaining a lighter, fibrous structure compared to fat-fried counterparts. Initially, MW samples exhibited some browning but appeared less compacted, suggesting that microwave energy penetrated the interior more uniformly without excessively drying the outer layer. Unlike the fat-fried samples, which turned darker and a bit rigid with time,

MW treated samples appeared to expand and develop a flaky texture at later stages, particularly at 150 and 180 s. This suggested that MW heating promoted structural breakdown through internal steam generation rather than surface dehydration, leading to a more aerated and fibrous texture (Srikanlaya & Therdthai, 2024). The final MW cooked sample at 180 s exhibited a rough and fragmented appearance, indicative of extensive internal water loss and protein restructuring, yet it did not reach the same extreme browning as fat-fried samples.

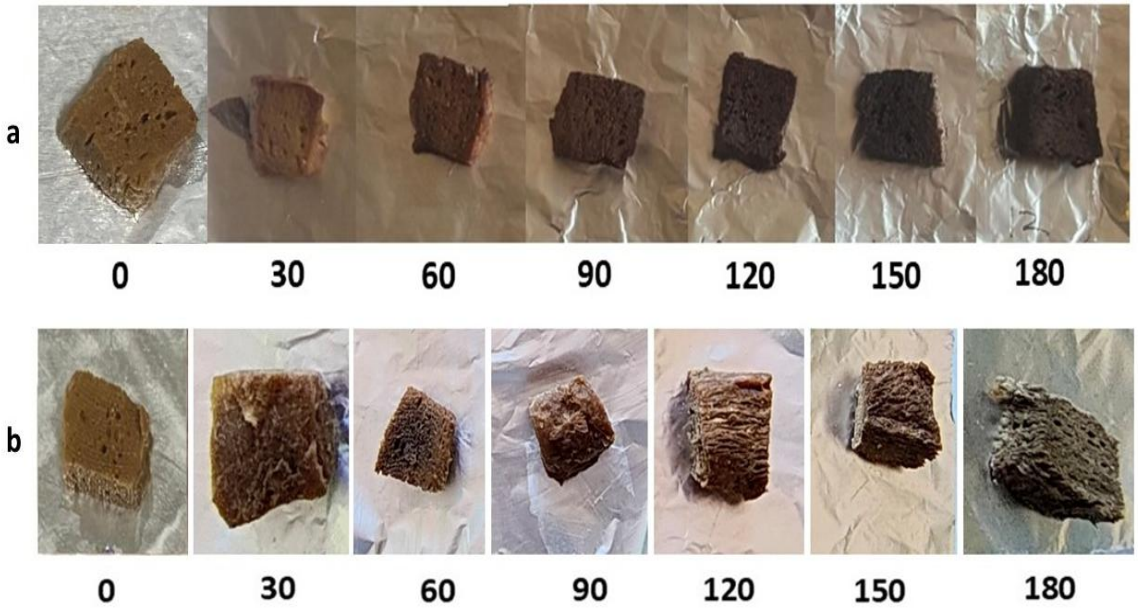

Figure 6.8: The appearance of the of texturized protein samples before cooking (0 s) and cooked samples after frying at 160 ℃ (a) and MW cooking at 900W (b) at different cooking times (30, 60, 90, 120, 150, 180 s)

Overall, fat-frying accelerated browning and surface hardening due to oil-mediated heat transfer, whereas MW cooking preserved more of the fibrous integrity while progressively dehydrating the sample uniformly. These visual differences provided critical insights into how cooking methods influenced the final sensory and functional properties of texturized proteins, with implications for food texture, digestibility, and consumer preference (Zhou et al., 2022).

6.3.12.2. Moisture content

An extensive comparative analysis of texturized protein samples revealed distinct

moisture retention patterns when subjected to fat-frying at 160 °C versus microwave cooking over a treatment duration spanning 0-180 s **(Table 6.21)**. The investigation started with identical initial moisture content values of 73.29% (w.b.) across all samples and the subsequent progression demonstrated marked divergences between the two cooking methodologies, with fat-fried samples consistently maintaining superior moisture retention during early processing stages. At the 30 s interval, fat-fried samples retained significantly ($p<0.05$) higher moisture content (56.12%) relative to microwave-treated counterparts (42.58%), a disparity that persisted through the 60 and 90 s timeframes, where fat-frying continued to exhibit enhanced moisture preservation (46.20% and 40.93%, respectively) compared to microwave cooking (39.83% and 36.81%). Interestingly, the differential narrowed considerably at the 120 and 150 s marks, with moisture content values approaching equivalence (27.63% and 25.21% for fat-frying; 28.20% and 26.03% for microwave treatment), suggesting a temporary convergence in dehydration kinetics between the methodologies.

Table 6.21: Moisture content values (% w. b.) for texturized protein samples obtained after fat-frying (160 °C) and microwave cooking (MW)

Time (s)	MC (% w.b.)	
	Frying at 160 °C	**MW (900W)**
0	73.29 ± 0.40^{aA}	73.29 ± 0.40^{aA}
30	56.12 ± 0.38^{bA}	42.58 ± 0.67^{bB}
60	46.20 ± 0.45^{cA}	39.83 ± 0.38^{cB}
90	40.93 ± 0.32^{dA}	36.81 ± 0.43^{dB}
120	27.63 ± 0.31^{eA}	28.20 ± 0.35^{eB}
150	25.21 ± 0.29^{fA}	26.03 ± 0.18^{fB}
180	23.11 ± 0.28^{gA}	14.46 ± 0.32^{gB}

Values are given as mean ± standard deviation (SD). a, b, c, d, e, f, g, A, B: Different lowercase and uppercase letter superscripts within the same column and rows, respectively, indicate statistically significant differences *($p<0.05$)*

However, the most pronounced distinction manifested at the 180 s terminal point, where microwave-processed samples experienced a precipitous decline in moisture content (14.46%), while fat-fried specimens maintained substantially higher hydration levels

(23.11%), thereby illuminating the fundamentally different moisture transfer mechanisms inherent to each technique (Chang et al., 2020). Fat-frying maintains higher moisture (23.11% vs 14.46% in microwaved samples), preserving juiciness and tenderness through an oil barrier that moderates moisture loss, though with increased fat content (Chang et al., 2020). Microwave cooking excels at rapid, uniform moisture reduction through volumetric heating, yielding consistent texture and better shelf stability. While fat-frying is preferred when moisture retention matters, microwave processing offers advantages in applications requiring dehydration, using less energy without oil, providing economic and nutritional benefits for specific uses (Thakur & Dalbhagat, 2023).

6.3.12.3. Cooking yield

The cooking yield (CY) values for texturized protein samples provide further insight into the impact of fat-frying and MW cooking on weight changes through moisture and fat loss or gain. **Table 6.22** represents cooking yield of the texturized protein samples obtained after fat-frying (160 ℃) and microwave (MW) cooking at 900W. As the cooking progressed, a clear distinction was observed, with fat-fried samples consistently demonstrating significantly ($p<0.05$) superior cooking yield and maintaining much of their original mass, whereas microwave-processed samples exhibited substantially diminished retention, indicating accelerated moisture volatilization during microwave exposure. This differential persisted through subsequent time points of 60 and 90 s, where fat-frying yielded significantly ($p<0.05$) higher CY values of 72.86% and 67.29% respectively, contrasted with the markedly lower microwave cooking yields of 63.18% and 49.82%, thereby illuminating the distinct mass transfer kinetics inherent to each thermal processing modality. The disparity became increasingly pronounced at extended durations, with fat-frying CY values declining to 58.00% and 55.64% at 120 and 150 s, while microwave cooking precipitated dramatically accelerated mass depletion, resulting in substantially reduced yields of 33.02% and 30.28% at corresponding intervals (Alugwu et al., 2022). The culmination of the experimental duration at 180 s revealed the most striking contrast, with microwave processing yielding a minimal retention of 26.94% compared to fat-frying's relatively stable 55.66%, underscoring the profound impact of processing methodology on final product mass. These observations can be mechanistically attributed to the fundamental distinctions in heat transfer phenomena.

Fat-frying establishes a hydrophobic surface barrier that impedes moisture loss, whereas microwave processing employs dielectric heating throughout the product matrix, facilitating rapid internal moisture mobilization and subsequent evaporative loss (Boukid et al., 2024). Fat-frying demonstrated clear superiority by maximizing yield and moisture retention, making it advantageous for applications where product economics and juiciness are paramount considerations (Asokapandian et al., 2020). The significantly higher terminal cooking yield at 180 s (55.66% versus 26.94% for microwave cooking) translates to substantially greater production efficiency and potentially enhanced organoleptic properties.

Table 6.22: Cooking yield (CY) values for texturized protein samples obtained after fat-frying (160 ℃) and microwave cooking (MW)

Time (s)	CY (%)	
	Frying at 160 ℃	**MW (900W)**
0	100.00^{aA}	100.00^{aA}
30	79.51 ± 0.38^{bA}	60.17 ± 0.33^{bB}
60	72.86 ± 0.41^{cA}	63.18 ± 0.42^{cB}
90	67.29 ± 0.37^{dA}	49.82 ± 0.29^{dB}
120	58.00 ± 0.33^{eA}	33.02 ± 0.45^{eB}
150	55.64 ± 0.26^{fA}	30.28 ± 0.28^{fB}
180	55.66 ± 0.34^{fA}	26.94 ± 0.31^{gB}

Values are given as mean ± standard deviation (SD). a, b, c, d, e, f, g, A, B: Different lowercase and uppercase letter superscripts within the same column and rows, respectively, indicate statistically significant differences *($p<0.05$)*

6.3.12.4. Cooking loss

Table 6.23 represents cooking loss of the texturized protein samples obtained after fat-frying (160 ℃) and microwave (MW) cooking at 900W. With the increase in cooking time, a sharp increase in cooking loss (CL) was observed, with MW cooking consistently showing significantly ($p<0.05$) higher losses than fat-frying. At 30 s, CL for the fat-fried samples was 20.49%, whereas MW cooking resulted in a much higher loss of 39.83%, indicating rapid dehydration and volatile compound release in MW treated samples. The disparity between the two methods remained evident at 60 and 90 s, with CL values for

fat-frying increasing to 27.14% and 32.71%, while MW cooking leads to losses of 36.81% and 50.17%, respectively.

Table 6.23: Cooking loss (CL) values for texturized protein samples obtained after fat-frying (160 ℃) and microwave cooking (MW)

Time (s)	CL (%)	
	Frying at 160 ℃	**MW (900W)**
0	0.00^{fA}	0.00^{gA}
30	20.49 ± 0.38^{eB}	39.83 ± 0.33^{fA}
60	27.14 ± 0.41^{dB}	36.81 ± 0.42^{eA}
90	32.71 ± 0.37^{cB}	50.17 ± 0.29^{dA}
120	42.00 ± 0.33^{bB}	66.97 ± 0.45^{cA}
150	44.36 ± 0.26^{aB}	69.71 ± 0.28^{bA}
180	44.34 ± 0.34^{aB}	73.05 ± 0.31^{aA}

Values are given as mean ± standard deviation (SD). a, b, c, d, e, f, g, A, B: Different lowercase and uppercase letter superscripts within the same column and rows, respectively, indicate statistically significant differences *($p<0.05$)*

During the interval of 120 to 150 s, MW cooked samples exhibited extreme weight loss, with CL values of 66.97% and 69.71%, respectively, whereas fat-fried samples exhibited more gradual reduction in the values, suggesting that the absorption of oil during fat-frying offset some of the moisture loss. By 180 s, MW cooking reaches the highest CL value of 73.05%, while fat-frying remained significantly ($p<0.05$) lower at 44.34%, reinforcing the conclusion that MW cooking induced greater mass reduction due to its rapid internal heating mechanism (Srikanlaya & Therdthai, 2024). The higher CL in MW cooking compared to fat-frying can be attributed to the different heat transfer mechanisms involved. In MW cooking, water molecules are excited internally, leading to accelerated evaporation and tissue breakdown (Li et al., 2019), whereas in fat-frying, the external oil layer forms a barrier that moderates water loss while simultaneously allowing some oil absorption, resulting in comparatively lower weight loss (Boukid et al., 2024). This difference has critical implications for food texture, nutrient retention, and overall product quality, suggesting that fat-frying may better preserve the structural integrity and juiciness of texturized protein samples compared to MW cooking.

6.3.12.5. Texture profile analysis (Hardness and springiness)

The mechanical properties of texturized protein samples, particularly hardness and springiness, provided critical insights into the textural changes induced by fat-frying at 160 ℃ and microwave (MW) cooking **(Table 6.24** and **Table 6.25)**. Hardness, a measure of the force required to deform the sample, underwent a drastic transformation in response to the cooking method and duration. Initially, prior to cooking, both the samples had hardness values of 614.9 g. However, as cooking progressed, a striking divergence emerged. After just first round of cooking at 30 s, MW cooked samples exhibited a significant ($p<0.05$) and extraordinary increase in hardness as the values jumped to 3025.72 g, whereas fat-fried samples showed a comparatively modest increase to 925.12 g.

Table 6.24: Hardness values for texturized protein samples obtained after fat-frying (160 ℃) and microwave cooking (MW)

	Hardness (g)	
Time (s)	**Frying at 160 ℃**	**MW (900W)**
0	614.9 ± 15.2^{gA}	614.9 ± 15.2^{gA}
30	925.12 ± 18.7^{fB}	3025.72 ± 48.2^{fA}
60	1341.43 ± 26.1^{eB}	5236.04 ± 91.1^{eA}
90	1576.95 ± 28.9^{dB}	24507.71 ± 436.8^{dA}
120	1908.82 ± 35.2^{aB}	75270.08 ± 890.6^{aA}
150	1833.91 ± 32.9^{bB}	71542.93 ± 648.4^{bA}
180	1676.44 ± 30.1^{cB}	31654.31 ± 386.1^{cA}

Values are given as mean ± standard deviation (SD). a, b, c, d, e, f, g, A, B: Different lowercase and uppercase letter superscripts within the same column and rows, respectively, indicate statistically significant differences *($p<0.05$)*

This trend intensified further, with MW cooking inducing an exponential rise in hardness, reaching a staggering 5236.04 g at 60 s and an extreme 24,507.71 g at 90 s, an almost fifteen-fold increase compared to fat-frying, which remained at a relatively mild value of 1576.95 g. The peak hardness values were observed at 120 s, where MW cooked samples attained an astonishing 75,270.08 g, far exceeding the hardness of fat-fried samples (1908.82 g). This suggested that MW cooking rapidly dehydrated the

samples, leading to excessive densification and a rigid structure (Taşkıran et al., 2020). Interestingly, beyond this peak, MW cooked samples became brittle and exhibited a decline in hardness at 150 and 180 s (71,542.93 g and 31,654.31 g, respectively), suggesting that excessive heating induced structural breakdown or brittleness. Conversely, fat-frying maintained a relatively stable trend, peaking at 120 s and exhibiting only a slight reduction thereafter, suggesting that oil absorption helped moderate textural changes and prevented extreme hardening (Alugwu et al., 2022; Ramírez-Flores et al., 2024).

Springiness, which is a measure of a sample's ability to return to its original shape after deformation, followed a distinct but complementary trend as shown in **Table 6.25**. Initially, both fat-fried and MW cooked samples exhibited identical springiness values of 0.97, indicating similar pre-cooking textural properties. However, as cooking progressed, a decline in springiness was observed in both treatments, with MW cooked samples experiencing a more pronounced reduction. At 30 s time period, the fat-fried samples retained a springiness of 0.90, whereas MW cooked samples dropped to 0.86, suggesting that MW cooking rapidly affected the elasticity of the protein matrix. This difference became more pronounced at 60 s, where MW cooking reduced springiness to 0.76, compared to 0.95 for fat-frying, reinforcing the hypothesis that MW induced dehydration severely impacted the material's flexibility and sample gotten significantly ($p<0.05$) brittle and broke after the applied force reached a certain limit. Anomalously, at 90 s, MW cooked samples exhibited an increase in springiness to 0.96, nearing their original state, while fat-fried samples remained unchanged at 0.97, hinting at possible transient structural changes due to MW induced internal moisture redistribution and case hardening which prevented excessive moisture loss and the moisture trapped inside kept the samples somewhat elastic (Nguyen et al., 2013; Tamsir et al., 2021). However, the drastic hardness values observed at this time point suggested that while MW cooked samples regained some elastic properties, they remained highly rigid overall. At 120 and 150 s, MW cooked samples exhibited a further decline in springiness (0.88 and 0.65, respectively), reflecting increasing stiffness and loss of flexibility, whereas fat-fried samples maintained relatively stable values (0.93 and 0.94), likely due to oil absorption mitigating excessive dehydration (Wilson et al., 2020). Interestingly, by 180 s, MW cooked samples unexpectedly regained their original springiness at 0.98, surpassing fat-fried samples (0.95). This suggested that prolonged MW exposure induced structural

changes that, counterintuitively, enhanced elasticity in later stages, possibly due to internal reorganization of protein fibers and moisture redistribution (Chumngoen et al., 2018).

Table 6.25: Springiness values for texturized protein samples obtained after fat-frying (160 ℃) and microwave cooking (MW)

	Springiness	
Time (s)	**Frying at 160 ℃**	**MW (900W)**
0	0.97 ± 0.003^{aA}	0.97 ± 0.003^{bA}
30	0.90 ± 0.005^{eA}	0.86 ± 0.002^{eB}
60	0.95 ± 0.003^{cA}	0.76 ± 0.001^{fB}
90	0.97 ± 0.003^{bA}	0.96 ± 0.002^{cB}
120	0.93 ± 0.004^{dA}	0.88 ± 0.002^{dB}
150	0.94 ± 0.003^{dA}	0.65 ± 0.001^{gB}
180	0.95 ± 0.004^{cA}	0.98 ± 0.002^{aA}

Values are given as mean ± standard deviation (SD). a, b, c, d, e, A, B: Different lowercase and uppercase letter superscripts within the same column and rows, respectively, indicate statistically significant differences *($p<0.05$)*

While fat-frying led to a gradual, controlled increase in hardness with moderate textural changes, MW cooking induced extreme fluctuations, drastically increasing hardness while intermittently altering springiness (Albert et al., 2009). These findings indicated that fat-frying provided a more balanced approach to textural modification, maintaining chewiness and flexibility, whereas MW cooking created highly rigid, brittle textures with potential textural instability over prolonged exposure (Wilson et al., 2020). This divergence was attributed to the different heat transfer mechanisms. In MW cooking, rapid volumetric heating led to severe dehydration, protein denaturation, and excessive densification, whereas fat-frying created a protective oil barrier that moderated water loss and prevented extreme hardening (Liu & Lanier, 2016; Asokapandian et al., 2020). These findings had critical implications for optimizing cooking techniques to achieve desirable textural properties in plant-based protein products, particularly in applications where controlled hardness and springiness were essential for consumer acceptability (Peñaranda et al., 2023).

6.3.12.6. Analysis of colour values (*L**, *a**, *b**)

The color characteristics, as fundamental quality indicators in food products influencing consumer perception and acceptance, underwent significant transformations in texturized protein samples when subjected to fat-frying at 160 °C **(Table 6.26)** and microwave (MW) cooking **(Table 6.27)** over various time intervals. The *L** value (lightness), decreased progressively in both cooking methods, indicating darkening attributed to Maillard reactions and caramelization processes (Kalogianni & Smith, 2013). In fat-fried samples, the initial *L** value of 51.01 dropped steadily to 33.23 at 180 s, demonstrating a substantial reduction in brightness and intensification of color as heat exposure continued. The most significant reductions occurred within the first 90 s, where *L** value declined sharply to 38.42, corresponding with protein denaturation, moisture removal, and the formation of brown pigments resulting from lipid oxidation reactions (Gruffat et al., 2021). In contrast, MW cooking resulted in a more gradual decline in lightness, with *L** value decreasing from 51.01 to only 43.62 over the same period. This slower rate of darkening in MW cooking suggested reduced surface browning compared to fat-frying, likely due to the absence of direct oil-mediated heat transfer and diminished Maillard reaction intensity at the surface (Park & Kim, 2021). Instead, MW cooking primarily affected internal moisture distribution, leading to structural modifications without inducing the same degree of surface pigmentation as observed in fat-frying (Noor Hidayati et al., 2021; Alugwu et al., 2022).

The *a** parameter, which measured redness, followed a pronounced declining trend in both treatments but at different rates. In fat-fried samples, *a** decreased from an initial value of 7.60 to a minimal 1.33 at 180 s **(Table 6.26)**, highlighting significant reductions in red pigmentation due to thermal degradation of natural color compounds, such as carotenoids and myoglobin-like proteins in plant-based analogues (Alugwu et al., 2022). The sharpest decline occurred within the first 90 s, with redness values dropping below 3.0, coinciding with the period of intense moisture loss and protein transformation. Interestingly, at 150 s, *a** briefly increased to 2.54 before declining again at 180 s, possibly due to variations in browning intensity and surface oil interactions affecting light reflectance (Nguyen et al., 2013). MW cooked samples exhibited a similar declining trend but retained higher *a** values throughout cooking **(Table 6.27)**. Starting at 7.60, *a** gradually decreased to 4.02 by 180 s, suggesting that MW heating preserved

red tones better than fat-frying, likely because MW energy penetrated volumetrically rather than focusing heat on the surface (Chang et al., 2020; Wereńska, 2023). The lower extent of direct browning reactions in MW cooking, coupled with less intense surface dehydration, contributed to the retention of higher *a** values compared to fat-frying. This distinction proved critical for achieving specific color targets in texturized protein products, where excessive browning or loss of red hues significantly impacted consumer appeal.

Table 6.26: Colour values (*L**, *a**, *b**) for texturized protein samples obtained after fat-frying (160 ℃)

Time (s)	Colour parameters		
	L*	***a****	***b****
0	51.01±0.24^{a}	7.60±0.20^{a}	12.1±0.24^{b}
30	43.59±0.32^{b}	5.68±0.28^{b}	14.17±0.25^{a}
60	40.35±0.29^{c}	4.35±0.26^{c}	6.78±0.27^{c}
90	38.42±0.26^{d}	2.42±0.22^{d}	2.13±0.25^{d}
120	36.99±0.21^{e}	1.49±0.20^{e}	0.41±0.23^{e}
150	34.94±0.18^{f}	2.54±0.17^{d}	2.39±0.22^{d}
180	33.23±0.15^{g}	1.33±0.14^{e}	-0.23±0.16^{f}

*L**: Lightness; *a**: Redness; *b**: Yellowness. Values are given as mean ± standard deviation (SD). a, b, c, d, e, f, g: Different lowercase letter superscripts within the same columns, indicate statistically significant differences *($p<0.05$)*

The *b** parameter, representing yellowness, exhibited unique behaviour in each cooking method. In fat-fried samples, *b** initially increased from 12.1 to 14.17 at 30 s, suggesting an initial intensification of yellow hues, possibly due to lipid absorption and early-stage Maillard reactions enhancing golden-brown tones (Alugwu et al., 2022). However, beyond 30 s, *b** decreased sharply, reaching -0.23 at 180 s, indicating a complete shift from yellow to darker brown or even blackened hues as heat exposure continued (Chang et al., 2020). This decline was associated with the formation of advanced Maillard reaction products and polymerization of browning compounds, which masked the initial yellowness and contributed to the final darkened appearance. In MW cooked samples, *b** followed a consistent downward trajectory from 12.1 to 2.66, maintaining positive values

throughout the process. The slower reduction in *b** compared to fat-frying implied that MW cooking did not induce the same level of surface browning or caramelization, likely because MW heating operated through internal water excitation rather than direct heat contact (Chang et al., 2020; Wereńska, 2023). The retention of some yellow hues in MW-cooked samples suggested that pigment degradation was less severe than in fat-fried samples, where direct oil exposure accelerated thermal breakdown (Park & Kim, 2021).

Table 6.27: Colour values (*L**, *a**, *b**) for texturized protein samples obtained after microwave cooking (MW)

Time (s)	Colour parameters		
	L*	***a****	***b****
0	51.01±0.24^{a}	7.60±0.20^{a}	12.1±0.24^{a}
30	46.94±0.28^{b}	6.29±0.13^{b}	6.44±0.11^{b}
60	46.92±0.32^{b}	5.80±0.10^{c}	5.33±0.09^{c}
90	46.77±0.23^{b}	5.27±0.11^{d}	4.52±0.05^{d}
120	45.98±0.27^{c}	4.84±0.06^{e}	2.95±0.03^{e}
150	43.74±0.19^{d}	4.75±0.08^{e}	2.89±0.06^{e}
180	43.62±0.31^{d}	4.02±0.02^{f}	2.66±0.02^{f}

*L**: Lightness; *a**: Redness; *b**: Yellowness. Values are given as mean ± standard deviation (SD). a, b, c, d, e, f: Different lowercase letter superscripts within the same columns, indicate statistically significant differences *($p<0.05$)*

Fat-frying induced rapid surface browning, significant darkening, and a pronounced reduction in redness and yellowness, primarily due to intense heat exposure, oil absorption, and slow dehydration. The sharp decline in *L**, coupled with the near disappearance of *b** by 180 s, suggested that fat-fried samples underwent extensive Maillard browning and caramelization, resulting in a darker, more visually complex product (Nguyen et al., 2013). In contrast, MW cooking led to a more controlled color change, with a slower decline in *L**, *a**, and *b**, indicating that the absence of direct oil-mediated heating moderated surface browning and pigment degradation (Alugwu et al., 2022; Wereńska, 2023). Products requiring a more pronounced golden-brown appearance benefited from fat-frying, whereas those requiring milder color changes or

the preservation of certain hues were better suited to MW cooking (Alugwu et al., 2022).

6.3.12.7. *In-vitro* protein digestibility (IVPD)

The *in-vitro* protein digestibility (IVPD) represents a critical parameter for evaluating the nutritional quality of texturized protein products, as it directly reflects the extent to which proteins are broken down and absorbed during digestion (Luo et al., 2018). The effects of fat-frying at 160 °C and microwave (MW) cooking on IVPD revealed a dynamic interplay between thermal processing and protein structure modifications **(Table 6.28)**. Initially, both samples had an identical IVPD value of 64.33%, but as cooking progressed, IVPD steadily increased in both treatments, demonstrating that heat application enhanced protein digestibility by disrupting protein-protein interactions, unfolding complex structures, and making peptide bonds more accessible to enzymatic hydrolysis (Alugwu et al., 2022).

Table 6.28: *In-vitro* protein digestibility (IVPD) values for texturized protein samples obtained after fat-frying (160 ℃) and microwave cooking (MW)

Time (s)	IVPD (%)	
	Frying at 160 ℃	**MW (900W)**
0	64.33 ± 0.30^{gA}	64.33 ± 0.30^{gA}
30	72.86 ± 0.42^{fA}	69.86 ± 0.26^{fB}
60	75.27 ± 0.47^{eA}	72.43 ± 0.41^{eB}
90	76.71 ± 0.50^{dA}	76.30 ± 0.33^{dA}
120	78.17 ± 0.45^{cB}	79.94 ± 0.46^{cA}
150	79.39 ± 0.58^{bB}	82.62 ± 0.51^{bA}
180	81.02 ± 0.52^{aB}	87.18 ± 0.48^{aA}

Values are given as mean ± standard deviation (SD). a, b, c, d, e, A, B: Different lowercase and uppercase letter superscripts within the same column and rows, respectively, indicate statistically significant differences *($p<0.05$)*

However, notable differences emerged in the rate and extent of improvement between fat-frying and MW cooking. After 30 s, fat-fried samples exhibited a significant (*$p<0.05$*) increase in IVPD to 72.86%, while MW cooked samples followed closely behind at 69.86%. As heating continued to 60 s, the gap between the two methods narrowed

slightly, with IVPD values rising to 75.27% in fat-fried samples and 72.43% in MW cooked samples. This divergence suggested that fat-frying, due to direct contact with hot oil, promoted faster protein denaturation and aggregation, potentially making the proteins more susceptible to enzymatic attack. MW cooking, on the other hand, achieved a similar effect but through volumetric heating, which penetrated the sample more evenly (Alugwu et al., 2022). By 90 s, both treatments yielded nearly identical IVPD values (76.71% for fat-frying and 76.30% for MW cooking), indicating that at this critical point, thermal effects on protein denaturation and digestibility reached a similar threshold regardless of cooking method (Park & Kim, 2021). This equilibrium suggested that heat-induced protein unfolding, cross-linking, and structural rearrangements balanced out between oil-based and MW heating, allowing for maximal enzymatic accessibility at this stage. However, as cooking extended beyond this point, MW cooking began to surpass fat-frying in enhancing IVPD. At 120 s, MW treated samples reached an IVPD of 79.94%, slightly exceeding the 78.17% observed in fat-fried samples. This pattern continued at 150 s, where MW cooking further improved digestibility to 82.62%, while fat-frying reached only 79.39%. The superior performance of MW cooking suggested that its volumetric heating mechanism continued to unfold proteins and disrupt intermolecular bonds more effectively, whereas fat-frying, which relied on surface heat transfer and oil absorption, may have started inducing secondary interactions such as Maillard cross-linking, which could potentially limit enzymatic accessibility (Luo et al., 2018). At 180 s, MW cooked samples exhibited the highest IVPD value of 87.18%, significantly ($p<0.05$) surpassing the 81.02% observed in fat-fried samples. MW cooking achieved superior results in the long term, likely due to its ability to prevent excessive surface hardening and cross-linking, which could reduce enzyme access. In contrast, prolonged fat-frying may have contributed to the formation of indigestible protein-lipid complexes or excessive surface browning, leading to localized protein degradation and a plateauing effect on IVPD improvement (Alugwu et al., 2022).

Overall, the results indicated that both fat-frying and MW cooking effectively enhanced protein digestibility by facilitating structural modifications that improved enzyme accessibility. However, the choice of cooking method played a crucial role in determining the extent of this improvement. Fat-frying provided rapid initial enhancement due to direct high-temperature exposure, making it advantageous for short-duration processing. However, prolonged frying introduced limiting factors such as

excessive surface hardening, Maillard reaction byproducts, and potential nutrient degradation (Park & Kim, 2021). In contrast, MW cooking offered a more sustained and progressive improvement in IVPD, ultimately yielding superior digestibility at extended cooking times.

6.3.12.8. Correlation analysis

Figure 6.9 represents the correlation heatmaps for fat-frying at 160 ℃ and microwave cooking, showing the differential impact of moisture content on critical quality parameters-cooking yield, textural hardness, lightness (*L**), and *in-vitro* protein digestibility (IVPD)-in texturized protein samples. During fat-frying at 160 ℃ **(Figure 6.9 a)**, a strong positive correlation was observed between moisture content and cooking yield (r=0.87, $p<0.01$), attributable to the concurrent processes of moisture evaporation and lipid absorption. Textural analysis demonstrated a moderate negative correlation between moisture content and hardness (r=-0.64, $p<0.05$), indicating progressive but controlled structural firmness development throughout the thermal treatment. The color parameters (*L** values), exhibited significant positive correlation with moisture content (r=0.79, $p<0.01$), suggesting that moisture reduction catalyzes non-enzymatic browning reactions, predominantly Maillard reactions (Tamsir et al., 2021). Functional quality, as measured by IVPD, displayed moderate improvement with decreasing moisture content (r=-0.59, $p<0.05$), indicating that controlled thermal denaturation facilitates enhanced proteolytic accessibility (Ohanenye et al., 2022). Conversely, microwave-processed samples exhibited markedly different correlation patterns **(Figure 6.9 b)**. A significantly steeper negative correlation was observed between moisture content and cooking yield (r=0.92, $p<0.001$), indicative of rapid moisture volatilization without compensatory mass incorporation (Sánchez-García et al., 2024). The correlation between moisture and hardness was notably pronounced (r=-0.88, $p<0.001$), suggesting excessive textural deterioration toward unpalatable rigidity. Although the *L** parameter correlation was less significant compared to fat-frying (r=0.61, $p<0.05$), the data still confirmed progressive darkening during thermal processing (Boukid et al., 2024). The most distinctive attribute of microwave processing was the strong negative correlation between moisture content and IVPD (r=-0.83, $p<0.001$), suggesting superior protein denaturation efficacy through volumetric and uniform thermal energy distribution (Park & Kim, 2021).

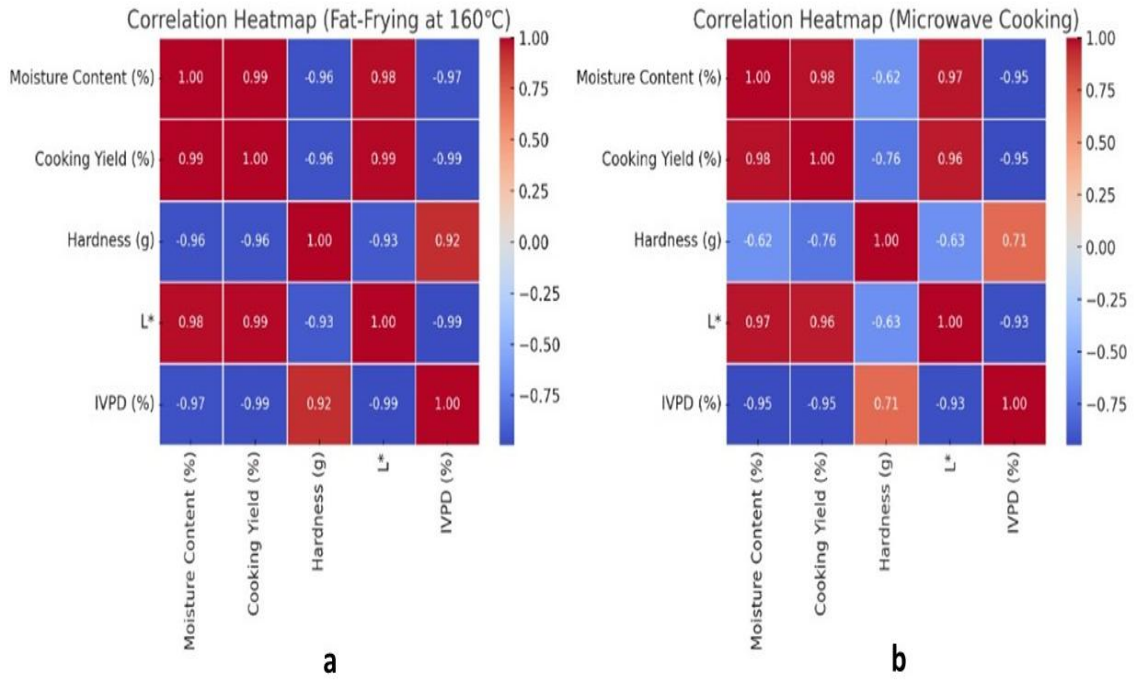

Figure 6.9: Correlation heatmaps for fat-frying at 160 ℃ and microwave cooking, showing the relationships between moisture removal and product quality attributes

Comparative evaluation of both thermal processing methodologies indicates that fat-frying at 160 ℃ maintains superior organoleptic and physical characteristics, including optimal textural development ($p<0.01$), enhanced mass retention ($p<0.01$), and controlled colorimetric progression ($p<0.05$) (Alugwu et al., 2022). While microwave processing demonstrated superior IVPD enhancement ($p<0.001$), the concomitant negative effects on texture and yield render it suboptimal for overall product quality (Li et al., 2019). Thus, fat-frying at 160 ℃ represents the optimal thermal processing modality for texturized protein products, balancing physicochemical stability and nutritional bioavailability.

6.4.Conclusion

The study investigated the moisture loss and fat absorption kinetics of texturized protein-based meat alternatives during deep-fat frying at three different temperatures (150 °C, 160 °C, 170 °C) and compared the quality parameters between conventional frying (160 °C) and microwave cooking (900W). The texturized protein had higher moisture and protein content compared to the reference sample. Frying resulted in progressive darkening and structural changes in the samples, with higher temperatures leading to

faster color development and moisture loss. Moisture content decreased significantly during frying, with the most rapid loss occurring within the first 60 s. Fat content increased with frying time, with higher temperatures resulting in greater fat absorption. Kinetic modelling revealed non-linear trends in moisture transfer and oil uptake rates, with 160 °C identified as the optimal temperature for moisture transfer. Cooking yield decreased during frying, with more pronounced changes at higher temperatures. Textural analysis showed significant increases in hardness and slight decreases in springiness during frying. Color analysis demonstrated a consistent decline in lightness, redness, and yellowness values, with total color change increasing over frying time. *In-vitro* protein digestibility improved significantly during frying, with higher temperatures resulting in greater digestibility. SEM analysis revealed microstructural changes, including increased porosity and heterogeneity, after frying. Correlation analysis highlighted complex relationships between mass transfer, heat transfer, and product quality parameters during the deep-fat frying process. Based on the comparative evaluation of thermal processing methods, fat-frying at 160 °C emerged as the superior approach for cooking texturized protein products, demonstrating significant advantages in preserving organoleptic and physical properties. The analysis therefore concluded that fat-frying at 160 °C represented the optimal thermal processing methodology for texturized protein products, successfully balancing physicochemical stability with nutritional bioavailability. This understanding can help manufacturers enhance product characteristics and streamline commercial development processes for these novel protein products and aim to provide insights for optimizing frying conditions in the large-scale production of texturized protein products.

References

Adedeji, A. A., Ngadi, M. O., & Raghavan, G. S. V. (2009). Kinetics of mass transfer in microwave precooked and deep-fat fried chicken nuggets. *Journal of food Engineering*, *91*(1), 146-153.

Ahmed, Z. A., & Mohammed, N. K. (2023, December). Influence of Multiple Deep-Frying Cycles on the Characteristics of Corn Oil and Acrylamide Content in French Fries. In *IOP Conference Series: Earth and Environmental Science*, *1262*(6), 062033.

Albert, Á., Varela, P., Salvador, A., & Fiszman, S. M. (2009). Improvement of crunchiness of battered fish nuggets. *European Food Research and Technology*, *228*, 923-930.

Alugwu, S. U., Okonkwo, T. M., & Ngadi, M. O. (2022). Effect of Cooking on Physicochemical and Microstructural Properties of Chicken Breast Meat. *European Journal of Nutrition and Food Safety*, *14*(11), 43-62.

Ang, J. F., & Miller, W. B. (1991). Multiple functions of powdered cellulose as a food ingredient. *Cereal Foods World*, *36*(7), 558-564.

Anjum, F. M., Naeem, A., Khan, M. I., Nadeem, M., & Amir, R. M. (2011). Development of texturized vegetable protein using indigenous sources. *Pakistan Journal of Food Science*, *21*(1-4), 33-44.

AOAC. (2006). Official Methods of Analysis, 18th ed. *Association of Official Analytical Chemists*, Arlington, *VA, USA*.

Arueya, G., Owosen, B., & Olatoye, K. (2017). Development of Texturized Vegetable Protein from Lima bean (*Phaseolus lunatus*) and African oil bean seed [*Pentaclethrama crophylla* (Benth)]: optimization approach. *Acta Universitatis Cinbinesis, Series E: Food Technology*, *21*(1).

Asokapandian, S., Swamy, G. J., & Hajjul, H. (2020). Deep fat frying of foods: A critical review on process and product parameters. *Critical Reviews in Food Science and Nutrition*, *60*(20), 3400-3413.

Bakr, Y., Al-Bloushi, H., & Mostafa, M. (2023). Consumer intention to buy plant-based meat alternatives: A cross-cultural analysis. *Journal of International Consumer Marketing*, *35*(4), 420-435.

Bhat, Z. F., Morton, J. D., Bekhit, A. E. D. A., Kumar, S., & Bhat, H. F. (2021). Thermal processing implications on the digestibility of meat, fish and seafood proteins. *Comprehensive Reviews in Food Science and Food Safety*, *20*(5), 4511-4548.

Bouchon, P. (2009). Understanding oil absorption during deep-fat frying. *Advances in Food and Nutrition Research*, *57*, 209-234.

Bouchon, P., & Dueik, V. (2018). Frying of foods. *Fruit Preservation: Novel and Conventional Technologies*, 275-309.

Boukid, F., Baune, M. C., Terjung, N., Francis, A., & Smetana, S. (2024). The 'meat-hybrid' concept: bridging the gap between texture, taste, sustainability and nutrition. *International Journal of Food Science and Technology*, *59*(11), 8645-8655.

Cao, Y., Sun, M., Huang, T., Zhu, Z., & Huang, M. (2024). Effects of heat sterilization on protein physicochemical properties and release of metabolites of braised chicken after in vitro digestion. *Food Chemistry*, *445*, 138670.

Castro-López, R., Mba, O. I., Gómez-Salazar, J. A., Cerón-García, A., Ngadi, M. O., & Sosa-Morales, M. E. (2023). Evaluation of chicken nuggets during air frying and deep-fat frying at different temperatures. *International Journal of Gastronomy and Food Science*, *31*, 100631.

Chang, C., Wu, G., Zhang, H., Jin, Q., & Wang, X. (2020). Deep-fried flavor: Characteristics, formation mechanisms, and influencing factors. *Critical Reviews in Food Science and Nutrition*, *60*(9), 1496-1514.

Chiang, J. H., Loveday, S. M., Hardacre, A. K., & Parker, M. E. (2019). Effects of soy protein to wheat gluten ratio on the physicochemical properties of extruded meat analogues. *Food Structure*, *19*, 100102.

Chumngoen, W., Chen, C. F., & Tan, F. J. (2018). Effects of moist-and dry-heat cooking on the meat quality, microstructure and sensory characteristics of native chicken meat. *Animal Science Journal*, *89*(1), 193-201.

Costa, R. M., & Oliveira, F. A. R. (1999). Modelling the kinetics of water loss during potato frying with a compartmental dynamic model. *Journal of Food Engineering*, *41*(3-4), 177-185.

Dana, D., & Saguy, I. S. (2006). Mechanism of oil uptake during deep-fat frying and the surfactant effect-theory and myth. *Advances in Colloid and Interface Science*, *128*, 267-272.

De Angelis, D., van der Goot, A. J., Pasqualone, A., & Summo, C. (2024). Advancements in texturization processes for the development of plant-based meat analogs: A review. *Current Opinion in Food Science*, *58*, 101192.

Delgado-Andrade, C., Seiquer, I., Haro, A., Castellano, R., & Navarro, M. P. (2010). Development of the Maillard reaction in foods cooked by different techniques. Intake of Maillard-derived compounds. *Food Chemistry*, *122*(1), 145-153.

Djekic, I. (2015). Environmental impact of meat industry–current status and future perspectives. *Procedia Food Science*, *5*, 61-64.

do Carmo, C. S., Rieder, A., Varela, P., Zobel, H., Dessev, T., Nersten, S., & Knutsen, S. H. (2023). Texturized vegetable protein from a faba bean protein concentrate and an oat fraction: Impact on physicochemical, nutritional, textural and sensory properties. *Future Foods*, *7*, 100228.

Dutta, D., & Sit, N. (2023). Comparison of properties of films prepared from casein modified by ultrasound and autoclave treatment. *Journal of Food Measurement and Characterization*, *17*(5), 5426-5439.

Flores-Jiménez, N. T., Ulloa, J. A., Urías-Silvas, J. E., Ramírez-Ramírez, J. C., Bautista-Rosales, P. U., & Gutiérrez-Leyva, R. (2022). Influence of high-intensity ultrasound on physicochemical and functional properties of a guamuchil *Pithecellobium dulce* (Roxb.) seed protein isolate. *Ultrasonics Sonochemistry*, *84*, 105976.

Gani, A., Wani, S. M., Masoodi, F. A., & Hameed, G. (2012). Whole-grain cereal bioactive compounds and their health benefits: A review. *Journal of Food Processing and Technology*, *3*(3), 1000146.

Gao, Y., Sun, Y., Zhang, Y., Sun, Y., & Jin, T. (2022). Extrusion modification: Effect of extrusion on the functional properties and structure of rice protein. *Processes*, *10*(9), 1871.

Gertz, C. (2014). Fundamentals of the frying process. *European Journal of Lipid Science and Technology*, *116*(6), 669-674.

Giami, S. Y., Adindu, M. N., Hart, A. D., & Denenu, E. O. (2001). Effect of heat processing on in vitro protein digestibility and some chemical properties of African breadfruit (*Treculia africana* Decne) seeds. *Plant Foods for Human Nutrition*, *56*, 117-126.

Gökmen, V., Palazoğlu, T. K., & Şenyuva, H. Z. (2006). Relation between the acrylamide formation and time-temperature history of surface and core regions of French fries. *Journal of Food Engineering*, *77*(4), 972-976.

Gruffat, D., Bauchart, D., Thomas, A., Parafita, E., & Durand, D. (2021). Fatty acid composition and oxidation in beef muscles as affected by ageing times and cooking methods. *Food Chemistry*, *343*, 128476.

Islam, J. (2023). Physicochemical Properties of Deep-Fried Surimi Fish Balls With β-Sitosterol-Loaded Oleogel and Citrus Peel Fiber (Master's thesis, North Carolina Agricultural and Technical State University).

Jang, J., & Lee, D. W. (2024). Advancements in plant-based meat analogs enhancing sensory and nutritional attributes. *NPJ Science of Food*, *8*(1), 50.

Kalogianni, E. P., & Smith, P. G. (2013). Effect of frying variables on French fry properties. *International Journal of Food Science and Technology*, *48*(4), 758-770.

Ketnawa, S., & Rawdkuen, S. (2023). Properties of texturized vegetable proteins from edible mushrooms by using single-screw extruder. *Foods*, *12*(6), 1269.

Kim, Y. J., Kim, J. H., Cha, J. Y., Kim, T. K., Jang, H. W., Kim, D. H., & Choi, Y. S. (2024). Quality characteristics of meat analogs through the incorporation of textured vegetable protein and *Tenebrio molitor* larvae in the presence of transglutaminase. *Food Science of Animal Resources*, *44*(5), 1028.

Kita, A. (2014). The effect of frying on fat uptake and texture of fried potato products. *European Journal of Lipid Science and Technology*, *116*(6), 735-740.

Krokida, M. K., Panagiotou, N. M., Maroulis, Z. B., & Saravacos, G. D. (2001). Thermal conductivity: Literature data compilation for foodstuffs. *International Journal of Food Properties*, *4*(1), 111–137.

Kumar, S., Nema, P. K., Kumar, S., & Chandra, A. (2022). Kinetics of change in quality parameters of khaja during deep-fat frying. *Journal of Food Processing and Preservation*, *46*(9), e16265.

Laugesen, S. B., Dethlefsen, S. L., Petersen, I. L., & Aaslyng, M. D. (2022). Texturized Vegetable Protein as a Source of Protein Fortification of Wheat Buns. *Foods*, *11*(22), 3647.

Le, H. M. Q., Tran, N. H. A., Nguyen, K. H., Nguyen, H. D., Tran, T. T. T., & Le, V. V. M. (2023). Frying of sliced shallot (*Allium ascalonium*): Product quality and kinetic models at different frying temperatures. *VNUHCM Journal of Engineering and Technology*, *6*(3), 2026-2034.

Lee, S., Jo, K., Jeong, H. G., Jeong, S. K. C., Park, J. I., Yong, H. I., & Jung, S. (2023). Higher protein digestibility of chicken thigh than breast muscle in an in vitro elderly digestion model. *Food Science of Animal Resources*, *43*(2), 305.

Li, M., McClements, D. J., Zhang, Z., Zhang, R., Jin, Z., & Chen, L. (2024). Influence of key component interactions in flour on the quality of fried flour products. *Critical Reviews in Food Science and Nutrition*, 1-12.

Li, S., Tang, S., Yan, L., & Li, R. (2019). Effects of microwave heating on physicochemical properties, microstructure and volatile profiles of yak meat. *Journal of Applied Animal Research*, *47*(1), 262-272.

Liu, S., Zhang, L., Guo, Y., Wang, M., Cai, H., Hong, P., & Lin, J. (2024). Study on quality characteristics, shelf-life prediction and frying mass transfer of breaded tilapia nuggets. *Heliyon*, *10*(17).

Liu, W., & Lanier, T. C. (2016). Rapid (microwave) heating rate effects on texture, fat/water holding, and microstructure of cooked comminuted meat batters. *Food Research International*, *81*, 108-113.

López, D. N., Ingrassia, R., Busti, P., Bonino, J., Delgado, J. F., Wagner, J., & Spelzini, D. (2018). Structural characterization of protein isolates obtained from chia (*Salvia hispanica* L.) seeds. *LWT-Food Science and Technology*, *90*, 396-402.

Lumanlan, J. C., Fernando, W. M. A. D. B., & Jayasena, V. (2020). Mechanisms of oil uptake during deep frying and applications of pre-drying and hydrocolloids in reducing fat content of chips. *International Journal of Food Science and Technology*, *55*(4), 1661-1670.

Luo, J., Taylor, C., Nebl, T., Ng, K., & Bennett, L. E. (2018). Effects of macro-nutrient, micro-nutrient composition and cooking conditions on in vitro digestibility of meat and aquatic dietary proteins. *Food Chemistry*, *254*, 292-301.

Mahmud, N., Islam, J., Oyom, W., Adrah, K., Adegoke, S. C., & Tahergorabi, R. (2023). A review of different frying oils and oleogels as alternative frying media for fat-uptake reduction in deep-fat fried foods. *Heliyon*, *9*(11).

Manjunatha, S. S., Mathews, A. T., & Patki, P. E. (2019). Modelling the kinetics of mass transfer and change in colour during deep fat frying of green peas (*Pisum sativum* L.) at different frying temperatures. *Heat and Mass Transfer*, *55*(11), 3087-3102.

McClements, D. J., & Grossmann, L. (2021). The science of plant-based foods: Constructing next-generation meat, fish, milk, and egg analogs. *Comprehensive Reviews in Food Science and Food Safety*, *20*(4), 4049-4100.

Mehta, U., & Swinburn, B. (2001). A review of factors affecting fat absorption in hot chips. *Critical Reviews in Food Science and Nutrition*, *41*(2), 133-154.

Mesías, M., & Delgado-Andrade, C. (2017). Melanoidins as a potential functional food ingredient. *Current Opinion in Food Science*, *14*, 37-42.

Miranda, M. L., & Aguilera, J. M. (2006). Structure and texture properties of fried potato products. *Food Reviews International*, *22*(2), 173-201.

Mohammadalinejhad, S., & Dehghannya, J. (2018). Effects of ultrasound frequency and application time prior to deep-fat frying on quality aspects of fried potato strips. *Innovative Food Science and Emerging Technologies*, *47*, 493-503.

Mondal, I. H., & Dash, K. K. (2017). Textural, color kinetics, and heat and mass transfer modeling during deep fat frying of Chhena Jhili. *Journal of Food Processing and Preservation*, *41*(2), e12828.

Morales, R., Martínez, K. D., Ruiz-Henestrosa, V. M. P., & Pilosof, A. M. (2015). Modification of foaming properties of soy protein isolate by high ultrasound intensity: Particle size effect. *Ultrasonics Sonochemistry*, *26*, 48-55.

Moreira, R. G., Sun, X., & Chen, Y. (1997). Factors affecting oil uptake in tortilla chips in deep-fat frying. *Journal of Food Engineering*, *31*(4), 485-498.

Moyano, P. C., & Pedreschi, F. (2006). Kinetics of oil uptake during frying of potato slices: Effect of pre-treatments. *LWT-Food Science and Technology*, *39*(3), 285-291.

Nguyen, V., Li, M., Khan, M. A., Li, C., & Zhou, G. (2013). Effect of cooking methods on tetracycline residues in pig meat. *Afr. J. Pharm. Pharmacol*, *7*(22), 1448-1454.

Ni, H., Deng, X., Li, Y., & Zou, Y. (2018). Moisture migration and quality changes of fried foods during deep-fat frying. *Food Science and Technology International*, *24*(6), 485-495.

Nikmaram, N., Leong, S. Y., Omman, R., Albadran, H. A., Galanakis, C. M., Farahnaky, A., & Barba, F. J. (2017). Effect of extrusion on the anti-nutritional factors of food products: An overview. *Food Control*, *79*, 62-73.

Noor Hidayati, R., Nurul Najihah, I., & Norazatul Hanim, M. R. (2021). Comparison of conventional frying and microwave frying of beef patty: effect on oil absorption, texture,

physical and chemical properties. *Food Research*, *5*(3), 399-405.

Ohanenye, I. C., Ekezie, F. G. C., Sarteshnizi, R. A., Boachie, R. T., Emenike, C. U., Sun, X., & Udenigwe, C. C. (2022). Legume seed protein digestibility as influenced by traditional and emerging physical processing technologies. *Foods*, *11*(15), 2299.

Oladejo, A. O., Ma, H., Qu, W., Zhou, C., Wu, B., Yang, X., & Onwude, D. I. (2017). Effects of ultrasound pretreatments on the kinetics of moisture loss and oil uptake during deep fat frying of sweet potato (*Ipomea batatas*). *Innovative Food Science and Emerging Technologies*, *43*, 7-17.

Palanisamy, M., Töpfl, S., Berger, R. G., & Hertel, C. (2019). Physico-chemical and nutritional properties of meat analogues based on Spirulina/lupin protein mixtures. *European Food Research and Technology*, *245*, 1889-1898.

Park, S. Y., & Kim, H. Y. (2021). Fried pork loin batter quality with the addition of various dietary fibers. *Journal of animal science and technology*, *63*(1), 137.

Pedreschi, F., & Zúñiga, R. N. (2009). Kinetics of quality changes during frying. Advances in deep-fat frying of foods, 81-113.

Pedreschi, F., Hernández, P., Figueroa, C., & Moyano, P. (2005). Modeling Water Loss During Frying of Potato Slices. *International Journal of Food Properties*, *8*(2), 289–299.

Peñaranda, I., Garrido, M. D., García-Segovia, P., Martínez-Monzó, J., & Igual, M. (2023). Enriched pea protein texturing: physicochemical characteristics and application as a substitute for meat in hamburgers. *Foods*, *12*(6), 1303.

Ramírez-Flores, I., Monroy-Rodríguez, I., & Gutiérrez-López, G. F. (2024). A Comparison of Traditional Oil and Hot-Air Frying with Respect to Composition, Morphological and Nutritional Characteristics of Fried Products. *Health-Promoting Food Ingredients During Processing*, 430-446.

Ran, X., Lin, D., Zheng, L., Li, Y., & Yang, H. (2023). Kinetic modelling of the mass and heat transfer of a plant-based fishball alternative during deep-fat frying and air frying

and the changes in physicochemical properties. *Journal of Food Engineering*, *350*, 111457.

Rimac-Brnčić, S., Lelas, V., Rade, D., & Šimundić, B. (2004). Decreasing of oil absorption in potato strips during deep fat frying. *Journal of Food Engineering*, *64*(2), 237-241.

Saguy, I. S., & Dana, D. (2003). Integrated approach to deep fat frying: Engineering, nutrition, health and consumer aspects. *Journal of Food Engineering*, *56*(2-3), 143-152.

Samard, S., & Ryu, G. H. (2019). A comparison of physicochemical characteristics, texture, and structure of meat analogue and meats. *Journal of the Science of Food and Agriculture*, *99*(6), 2708-2715.

Samard, S., Maung, T. T., Gu, B. Y., Kim, M. H., & Ryu, G. H. (2021). Influences of extrusion parameters on physicochemical properties of textured vegetable proteins and its meatless burger patty. *Food Science and Biotechnology*, *30*, 395-403.

Sánchez-García, J., Muñoz-Pina, S., García-Hernández, J., Heredia, A., & Andrés, A. (2024). Volatile profile of quinoa and lentil flour under fungal fermentation and drying. *Food Chemistry*, *430*, 137082.

Sanz, T., Primo-Martín, C., & Van Vliet, T. (2007). Characterization of crispness of French fries by fracture and acoustic measurements, effect of pre-frying and final frying times. *Food Research International*, *40*(1), 63-70.

Simpson, R., Jaques, A., Nuñez, H., Ramirez, C., & Almonacid, A. (2013). Fractional calculus as a mathematical tool to improve the modeling of mass transfer phenomena in food processing. *Food Engineering Reviews*, *5*, 45-55.

Sivaranjani, S., Joshi, T. J., Singh, S. M., & Rao, P. S. (2024). A comprehensive review of the mechanism, changes, and effect of deep fat frying on the characteristics of restructured foods. *Food Chemistry*, 139393.

Soorgi, M., Mohebbi, M., Mousavi, S. M., & Shahidi, F. (2012). The effect of methylcellulose, temperature, and microwave pretreatment on kinetic of mass transfer

during deep fat frying of chicken nuggets. *Food and Bioprocess Technology*, *5*, 1521-1530.

Srikanlaya, C., & Therdthai, N. (2024). Characterization of Plant-Based Meat Treated with Hot Air and Microwave Heating. *Foods*, *13*(17), 2697.

Tamsir, M. M., Ramli, N. S., Ab-Rashid, N. K. M., Shukri, R., & Ismail-Fitry, M. R. (2021). Comparison of boiling, steaming, air frying, deep-frying, microwaving and oven-cooking on quality characteristics of keropok lekor (Malaysian fish sausage). *Malaysian Applied Biology*, *50*(3), 77-85.

Taşkıran, M., Olum, E., & Candoğan, K. (2020). Changes in chicken meat proteins during microwave and electric oven cooking. *Journal of Food Processing and Preservation*, *44*(2), e14324.

Thakur, A., & Dalbhagat, C. G. (2023). Fundamentals, Methodologies, and Developments in Food Frying. In *Frying Technology* (pp. 57-90). CRC Press.

Vélez-Ruiz, J. F., Sosa-Morales, M. E., & López-Malo, A. (2002). Heat transfer during deep-fat frying of chicken strips. *Journal of Food Process Engineering*, *25*(3), 117-133.

Wang, C., Su, G., Wang, X., & Nie, S. (2019). Rapid assessment of deep-frying oil quality as well as water and fat contents in French fries by low-field nuclear magnetic resonance. *Journal of Agricultural and Food Chemistry*, *67*(8), 2361-2368.

Wang, L., Zhang, M., & Liu, Z. (2024). Oil uptake mechanisms during deep-fat frying: Relationship with surface phenomena and quality parameters. *Food Structure*, *31*, 100257.

Wereńska, M. (2023). Comparative study on the effects of sous-vide, microwave cooking, and stewing on functional properties and sensory quality of goose meat. *Poultry Science*, *102*(11), 103064.

Wilson, A., Anukiruthika, T., Moses, J. A., & Anandharamakrishnan, C. (2020). Customized shapes for chicken meat–based products: Feasibility study on 3D-printed nuggets. *Food and Bioprocess Technology*, *13*, 1968-1983.

Xia, S., Song, J., Ma, C., Hao, T., Hou, Y., Shen, S., & Jiang, X. (2023). Effects of moisture content and processing temperature on the strength and orientation regulation of fibrous structures in meat analogues. *Food Hydrocolloids*, *145*, 109113.

Xue, J., & Ngadi, M. (2006). Effect of carboxymethylcellulose on thermal properties of batter systems formulated with different flour combinations. In *2006 ASAE Annual Meeting* (p. 1). American Society of Agricultural and Biological Engineers.

Yang, D., Wu, G., Li, P., Zhang, H., & Qi, X. (2019). Comparative analysis of the oil absorption behavior and microstructural changes of fresh and pre-frozen potato strips during frying via MRl, SEM, and XRD. *Food Research International*, *122*, 295-302.

Zhou, H., Vu, G., Gong, X., & McClements, D. J. (2022). Comparison of the cooking behaviors of meat and plant-based meat analogues: Appearance, texture, and fluid holding properties. *ACS Food Science and Technology*, *2*(5), 844-851.

Ziaiifar, A. M., Achir, N., Courtois, F., Trezzani, I., & Trystram, G. (2008). Review of mechanisms, conditions, and factors involved in the oil uptake phenomenon during the deep-fat frying process. *International Journal of Food Science and Technology*, *43*(8), 1410-1423.